5-2020

Photocatalytic Carbon Dioxide Reduction with Zinc(II) Dipyrrin Photosensitizers and Iron Catalyst

Senan Rasheed
East Tennessee State University

Photocatalytic Carbon Dioxide Reduction with Zinc(II) Dipyrrin Photosensitizers and Iron Catalyst

---

A thesis

presented to

the faculty of the Department of Chemistry

East Tennessee State University

In partial fulfillment

of the requirements for the degree

Master of Science in Chemistry

---

by

Senan Adnan Rasheed

May 2020

Dr. Catherine E. McCusker

Dr. Dane W. Scott

Dr. Greg Bishop

Keywords:

Photocatalysis, CO^2 reduction, iron catalyst, Photosensitizer, zinc dipyrrin

ABSTRACT

Photocatalytic Carbon Dioxide Reduction with Zinc(II) Dipyrrin

Photosensitizers and Iron Catalyst

by

Senan Adnan Rasheed

Much of the energy used in the United States is obtained from petroleum, natural gas, and coal. Photocatalytic CO_2 reduction can be used to transform CO_2 to fuels. Input of energy is required, and the sun can provide the energy for this transformation. Photosensitizer, catalyst, and electron donor are required for photocatalytic CO_2 reduction.

Due to lack of earth-abundant sensitizers, zinc dipyrrin complexes were synthesized by previous group members and have been used as photosensitizers in this research. The ground and excited state electrochemical properties of two zinc dipyrrin complexes were determined in polar and nonpolar solvents and the measured potentials were used to match the zinc sensitizers with an energetically appropriate iron porphyrin catalyst and a benzyl thiol electron donor. Lastly, CO_2 gas was used for the reduction of CO_2 by photocatalysis with zinc photosensitizers, iron catalyst and electron donor. The products formed in headspace were analyzed by GC.

ACKNOWLEDGMENTS

In the name of Allah, the Most Gracious, the Most Merciful

I do offer my thanks and sincere appreciation to my committee chair, Dr. Catherine McCusker, for the guidance, learning opportunities, and support in this research. I am thankful to Dr. Dane W. Scott and Dr. Greg Bishop for their valuable advice, encouragements, and for being part of my committee.

I am thankful to ETSU Office of Research and Sponsored Programs and Donors of the American Chemical Society Petroleum Research for their financial support in this research. I would like to thank the faculty and staff of the Department of Chemistry ETSU.

Finally, my deepest gratitude to my parents, loving wife and two years old son, and friends for their support, caring, and prayer during my studies.

TABLE OF CONTENTS

LIST OF TABLES

LIST OF FIGURES

LIST OF ABBREVIATIONS

Abbreviation	Name
BODIPY	Boron Difluoride Dipyrrinato
CE	Counter electrode
CO	Carbon monoxide
CO_2	Carbon dioxide
CV	Cyclic voltammetry
DCM	Dichloromethane
$FeF_{20}TPPCl$	5,10,15,20-tetrakis(pentafluorophenyl)-21H,23H porphyriniron(III) chloride
GC	Gas Chromatography
HS	Headspace
ISC	Intersystem crossing
LOD	Limit of detection
LOQ	limit of quantification
PS	Photosensitizer
RE	Reference electrode
$TBAPF_6$	Tetrabutylammonium hexafluorophosphate
TCD	Thermal conductivity detector
THF	Tetrahydrofuran
TON	Turnover number
WE	Working electrode
ZnDPY	Bis(1,3,7,9-tetramethyl-5-mesityldipyrrinato)zinc(II)

ZnIDPY	Bis(2,8-diiodo-1,3,7,9- tetramethyl-5-mesityldipyrrinato)zinc(II)

CHAPTER 1: INTRODUCTION

Project Overview and Objective

An estimated of 80% of the energy used in the United States and around the globe is obtained from petroleum, natural gas, and coal as shown in Figure 1. Carbon dioxide (CO_2) emissions from fossil fuel consumption have increased about 29% between 2000 and 2008 in the concentration of atmospheric CO_2.[1,2] Consumption of fossil fuel energy still dominates because it is cheaper, higher in energy efficiency and more readily available for usage as compared to other sources.[3] However, the issue with these carbon-based energy sources is that they are non-renewable. In order to reduce or control the rising level of carbon dioxide in the atmosphere, consumption of carbon-based energy source must be reduced, and they must be replaced with carbon-neutral energy sources that are consumable.[4]

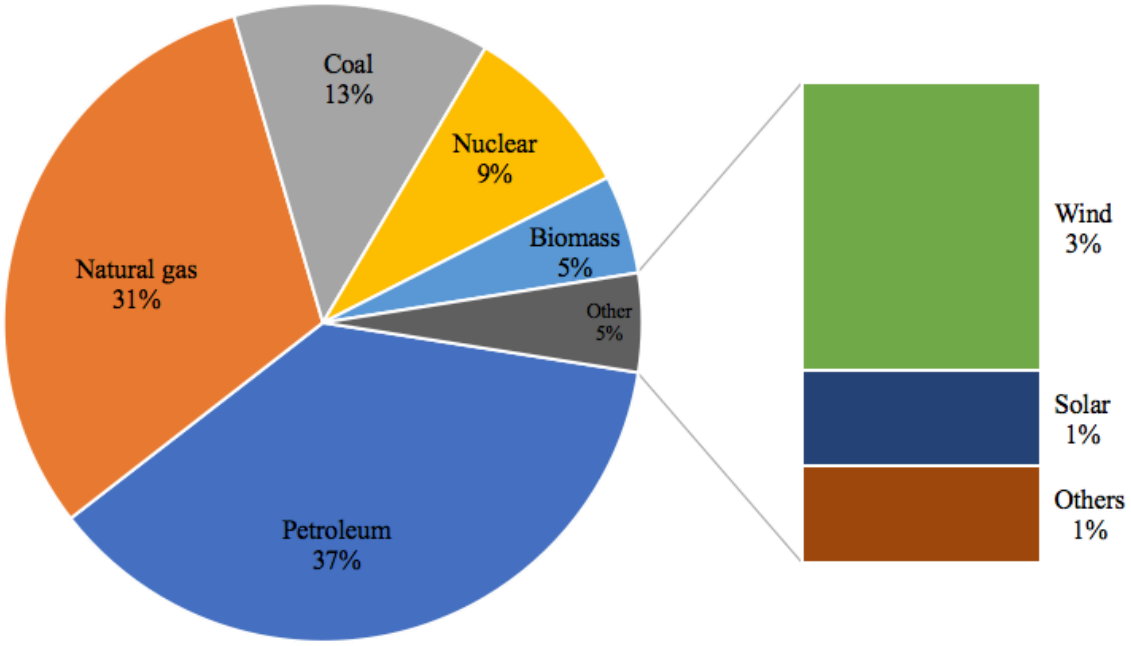

Figure 1. Estimated United States energy consumption in 2018.[5]

Carbon-neutral energy sources signifies the conversion of carbon dioxide into less harmful and more useful products in contrast to carbon energy sources. One of the ways to utilize these carbon-neutral energy sources is by photocatalytic reduction of carbon dioxide that may provide a solution to the dependence on non-renewable carbon energy sources. Photochemical reduction of carbon dioxide using a clean, renewable, and free source of energy such as sunlight instead of electricity is a promising pathway to accomplish the conversion of carbon dioxide without any additional source of energy. To achieve this purpose, molecular based photocatalytic reduction of carbon dioxide has been reinvestigated in the last few years.[6–9]

In this process, the carbon dioxide waste produced from burning fossil fuels can be catalytically transformed into new sources of energy such as methane gas, making these fuels a more renewable energy option.[10] However, reduction of carbon dioxide is an energy-demanding process because of the high stability of the carbon dioxide molecule.[11] As a result, an input of energy is required for this process. One of the possible sources for the required energy is sunlight. Furthermore, a photosensitizer may be incorporated to the reaction to make the process more efficient.

Photocatalysis with Zinc(II) Dipyrrin Sensitizers

A photosensitizer is a molecule that initially absorbs radiation, causing a photochemical or photophysical alteration in another molecule.[12] A photosensitizer is an important coreactant in the process of photocatalytic carbon dioxide reduction.[10] Its role is basically to collect light to initiate the chemical process.[11] In a study conducted by Bonin et al., the presence of a photosensitizer was found to provide several advantages as compared to its absence in their photocatalysis chemical reaction using iron-based homogenous catalyst.[13] One of the advantages they found is that photosensitizer lowers irradiation energy by shifting the absorption into the

visible region. Another advantage is that photosensitizer increases the efficiency of the process by boosting the final step for carbon monoxide (CO) formation, such as the reduction of CO_2-catalyst stripped by radical anion photosensitizer that acts as electron donor. Moreover, photosensitizer reduces the catalyst to its active state. Lastly, photosensitizer separates the light absorption from the catalysis itself to prevent the catalyst from playing both roles as a photosensitizer and/or catalyst for CO_2 reduction.[11]

A successful photosensitizer should form a long-lived triplet excited state longer than a microsecond and must be energetically capable of reducing the catalyst to drive the reduction of carbon dioxide. In order to carry out a photocatalytic carbon dioxide reduction, a photosensitizer for light absorption, sacrificial electron donor, and a catalyst are required. It is highly recommended that both photosensitizer and catalyst are made from Earth-abundant materials if the technology were to be applied on a large scale.[10] In the literature on carbon dioxide reduction catalysts, various studies have been devoted to study metal-based molecular catalysts for either electrochemical and photochemical reduction of carbon dioxide.[14–16] There are many examples of reduction catalysts that include the first-row transition metals such as those shown in Figure 3. However, examples of Earth-abundant photosensitizers, especially those used with carbon dioxide reduction catalysis, are far more rare.[13,17–19] With that, the aim of this study is to test the ability of zinc photosensitizers to sensitize photocatalytic carbon dioxide reduction with one of many known carbon dioxide reduction catalysts.

In the artificial photosynthesis research, photocatalysis of carbon dioxide to form CO is considered an important reaction to address the issue of global warming and the unavailability of energy and carbon resources.[20] In previous research studies, many metal-polypyridine complexes incorporating in photosensitizers have been used in various photocatalytic systems for carbon

dioxide reduction.[21] In particular, both ruthenium and iridium are popular in fundamental studies and applications as photosensitizers due to their advanced photochemical, redox properties, and to their stability against photodecomposition.[22,23] However, these metals are very rare and expensive and the use of first-row transition metal as photosensitizer has not been widely studied. As a result, a new photosensitizer based on earth-abundant transition metals is needed due to their low cost and to their abundance in earth's crust, as illustrated in Figure 2.[24]

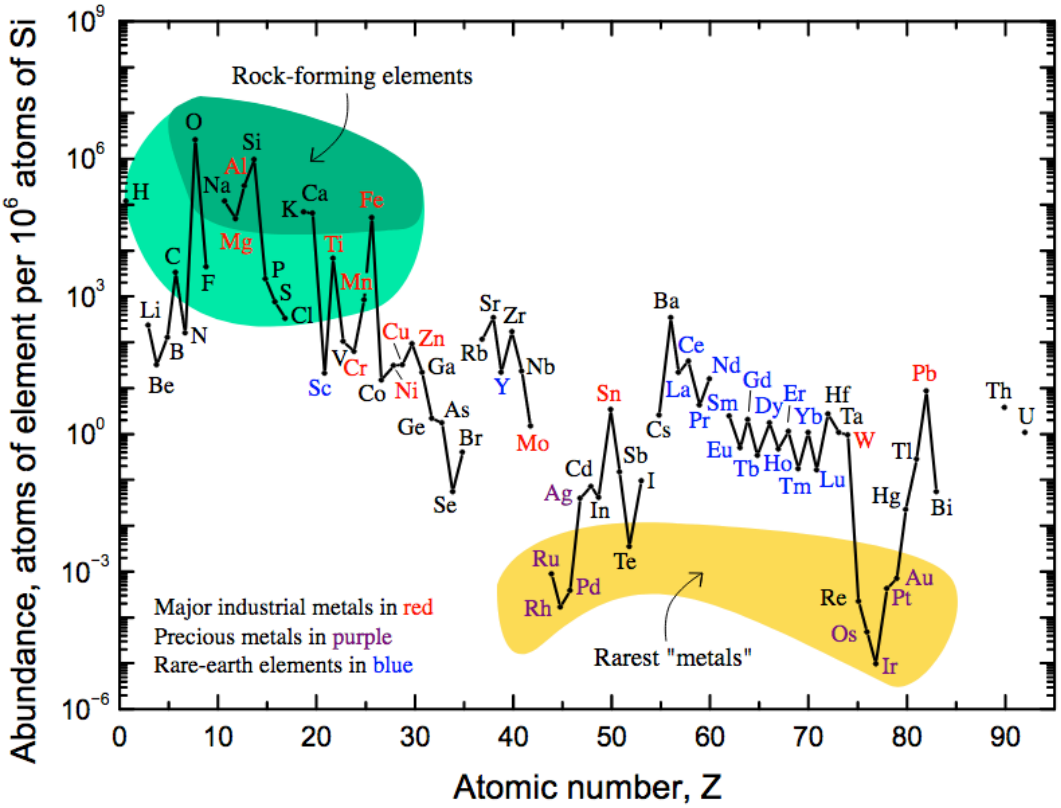

Figure 2. Abundance of elements in the earth's crust. Purple highlights some of the metals that most commonly used as photosensitizers. Red highlights major industrial metals including the first-row transition metals.[24]

Carbon Dioxide Reduction Catalysts Incorporating Earth-abundant Materials

The reduction of carbon dioxide can be accomplished in a variety of multielectron reductions reaction coupled with proton transfers. These reactions can lead to compounds such as carbon monoxide or can lead to formation of hydrocarbons (mixing carbon monoxide and

hydrogen molecule using the Fisher-Tropsch process)[25–27] ($2e^-$, $2H^+$), formaldehyde ($4e^-$, $4H^+$), methanol ($6e^-$, $6H^+$), and even methane ($8e^-$, $8H^+$).[8]

Due to the high stability of CO_2 molecule, a large input of energy is required for the transformation to carbon monoxide due to its highly oxidized state.[10] Carbon dioxide can be reduced to carbon monoxide by a reaction where there is a transfer of two electrons and two protons. Looking at Table 1[10] , this reaction is favorable at low potentials compared to the one electron reduction in water that occurs at very negative potentials (-1.90 V vs. normal hydrogen electrode at pH 7).[28]

Examples of the reduction of CO_2 shown in Table 1 are slow to occur without a catalyst. As a result, an energetically appropriate catalyst is required to efficiently increase the reaction rate for each of those reactions.[13] As mentioned above, many studies have been devoted to examining the metal-based molecular catalysts for both electrochemical and photochemical reduction of carbon dioxide. However, most of them are based on redox catalysts containing precious metals such as rhenium[29–31] or ruthenium.[32–34] These reduction catalysts can be either electrocatalytic or sensitized by ruthenium or iridium-based photosensitizers.

Table 1. Standard Potentials for Various CO_2 Reductions Reactions at pH 7.[10]

$CO_2 + 2H^+ + 2e^- \rightleftharpoons CO + H_2O$	$E^0 = -0.53$ V
$CO_2 + 2H^+ + 2e^- \rightleftharpoons HCO_2H$	$E^0 = -0.61$ V
$CO_2 + 4H^+ + 4e^- \rightleftharpoons HCHO + H_2O$	$E^0 = -0.48$ V
$CO_2 + 6H^+ + 6e^- \rightleftharpoons CH_3OH + H_2O$	$E^0 = -0.38$ V
$CO_2 + 8H^+ + 8e^- \rightleftharpoons CH_4 + 2H_2O$	$E^0 = -0.24$ V
$CO_2 + e^- \rightleftharpoons CO_2^{\cdot -}$	$E^0 = -1.90$ V

An alternative to the precious metal catalyst, earth abundant metals catalyst shown in Figure 3 such as cobalt[35,36] nickel[37,38] and iron[39,40] that have great efficiency and good chemical stability and they are also capable of reducing carbon dioxide to carbon monoxide both electrochemically and photochemically.[41] First-row transition metals complexes such as iron porphyrin and its derivatives are among the earth-abundant homogenous catalysts that offer great combination of efficiency and chemical stability for the reduction of carbon dioxide when an electron is transferred from the electrode or photosensitizer.[13,42,43] As Bonin et al. states, iron porphyrin and its derivatives have good performances in reduction of carbon dioxide to carbon monoxide with turnover number (TON) of up to 30 and have catalytic selectivity of up to 85%.[11] However, 30 is not very high TON for a catalyst compared to the TON of 98,000 that was recorded for rare metal-based catalyst such Ru and Re.[6,38] TON is the maximum number of moles of substrate that can be converted by a mole of catalyst before the reaction becomes inactive.

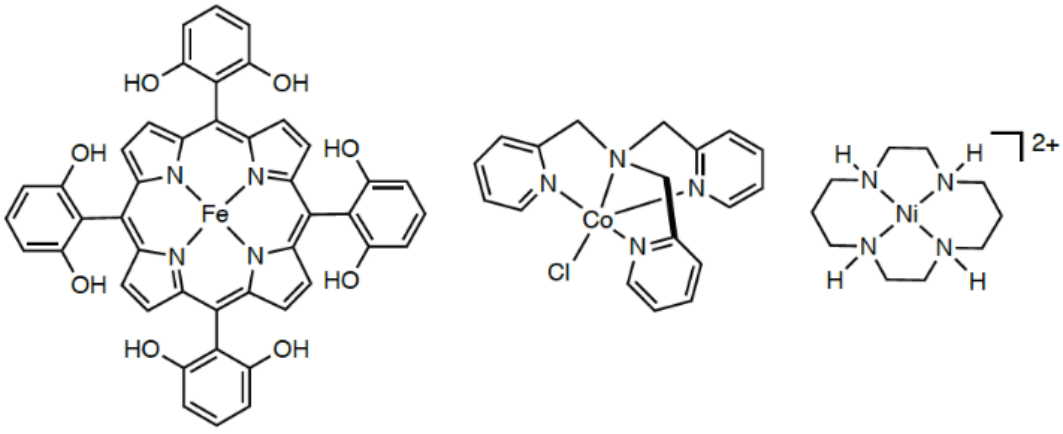

Figure 3. Examples of carbon dioxide reduction catalysts incorporating first-row transition metals.[35–40]

This research study will focus on discrete molecular photosensitizers and catalysts and the bimolecular chemistry between them, allowing a modular testing approach. For instance, multiple catalysts can be used to scan a single photosensitizer without modifying a covalently linked system. With this, the sensitizer and catalyst are not covalently bonded, and the excited sensitizer must be sufficiently long-lived (~µs) to undergo electron transfer to reduce the catalyst before the excited sensitizer relaxes back to its ground state. These requirements are available in the triplet excited state due to a forbidden transition that results in a slow relaxation process back to the singlet ground state resulting in a long-lived excited state.[44] Mechanistically, reduction of CO_2 by photochemical system consists of four different electron-transfer steps in the reductive quenching cycle of CO_2, as shown in Figure 4.[11]

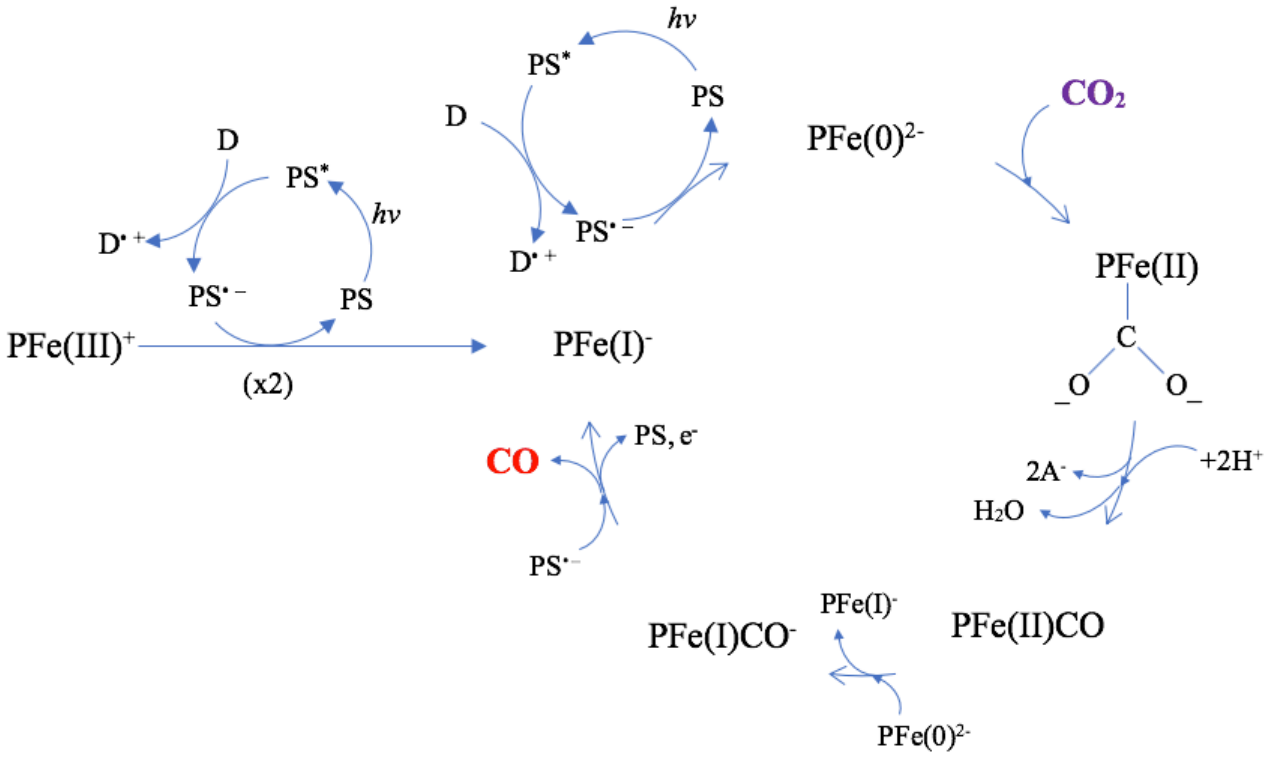

Figure 4. Photocatalysis reductive quenching cycle for the conversion of CO_2 to CO. PFe represents porphyrin. D represents electron donor. PS represents photosensitizer.[11,45]

To initiate the process in Figure 4, the photosensitizer (PS) must first be excited by absorption of visible light. Then, the excited state of the photosensitizer (PS^*) is first reductively quenched by the electron donor. As a result, generation of radical $PS^{\bullet -}$ acts as powerful reductant that can reduce the iron catalyst to its active state $PFe(0)^{2-}$. The radical anion of $PS^{\bullet -}$ can react with iron catalyst $PFe(III)^{+}$ in a total of three consecutive steps to yield a catalytically active catalyst $PFe(0)^{2-}$. Then, the available carbon dioxide in the latter can undergo adduct formation with the active catalyst to successfully form $[PFe(II) - CO_2]^{2-}$ by single carbenoid resonant form, as shown in Figure 5b. In Figure 5c and 5d, protonation of carbenoid complex can be accomplished by addition of two successive weak acid molecules (HA). A weak acid is required to stabilize the intermediate $[PFe(II) - CO_2]^{2-}$ by hydrogen bonding. This is followed by adduct of one CO bond that leads to a stable $PFe(II)CO$ complex as shown in Figure 5e. In Figure 5f and 5g, $PFe(I)^{-}$ is regenerated when $PFe(II)CO$ is reduced by $PFe(0)^{2-}$. The cleavage of $PFe(I)CO^{-}$ in the final step of Figure 5g to form CO is accomplished by the radical $PS^{\bullet -}$ that acts as an electron donor. The product of $PFe(I)^{-}$ in Figure 5f and 5g can be further reduced to form the active catalyst $PFe(0)^{2-}$, as shown in Figure 5a.

To design a sensitizer for photochemical carbon dioxide reduction, there are other principles to follow. Importantly, the sensitizer must absorb visible light to avoid decomposition of components in solution that might result from absorption lower wavelength. Less material can be used to absorb the same amount of light if the sensitizer has a high visible absorption cross-section and extinction coefficient. Furthermore, both CO_2 reduction catalyst and photosensitizer should be highly soluble in a polar solvent, such as THF, otherwise heterogenous catalysis reaction is involved instead of photocatalysis.[44] Additionally, reversible electrochemistry is

important as well so that the excited sensitizer can regenerate over many the cycles of oxidation and reduction without being decomposed.

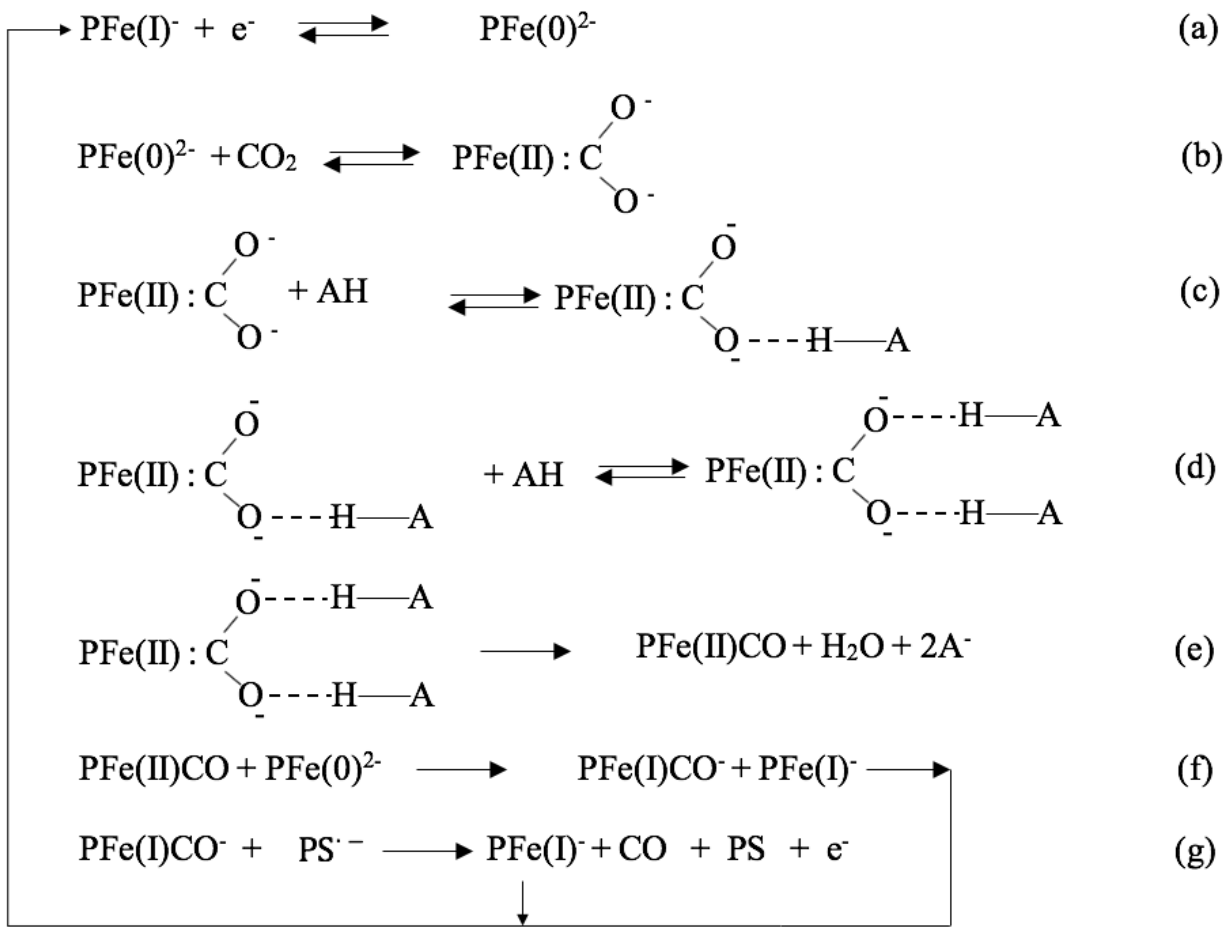

Figure 5. Equations (a) through (g) are represent the intermediate step for the reduction of carbon dioxide to form CO. AH represents the acid.[45]

Dipyrromethenes and pyrromethenes are commonly known as dipyrrin ligand that are capable of forming complexes that have potential to meet the above criteria for photosensitizers, as shown in Figure 6.[46] Dipyrrin ligands have the intense visible absorption properties of the porphyrins, while being more synthetically accessible.

Of the dipyrrin family, boron dipyrromethene (BODIPY) complexes are the most studied due to their high fluorescence quantum yields.[47–49] Unfortunately, BODIPY dyes have poor intersystem crossing (ISC) efficiency, causing them to have a high fluorescence quantum yields. Because of the poor ICS, BODIPY dyes also have a short excited state lifetimes of picoseconds to nanosecond.

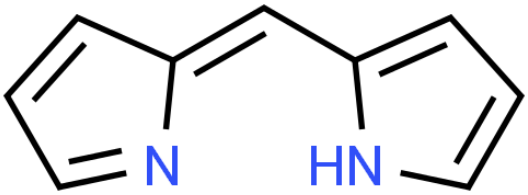

Figure 6. Structure of 2-(2H-pyrrol-2-ylidenemethyl)-1H-pyrrole also known as dipyrrin.[50]

Transition metal dipyrrin complexes are known, however they are less studied than their BODIPY counterparts. When the dipyrrin ligand is coordinated to a third-row transition metal, phosphorescence is observed, indicating the formation of a triplet excited state.[51,52] First-row transition metal complexes of dipyrrin ligands are also known and are often used in coordination polymers.[53–55] At room temperature in a solid state and in polar solvent, several zinc(II) bis-dipyrrin complexes form a long-lived triplet states.[56,57] Electrochemical and photochemical properties for zinc dipyrrin complexes have been studied by researchers.[58,59] However, zinc dipyrrin complexes have never been used as photosensitizers. As a result, this research will focus on using metal complexes involving zinc, a first-row transition metal, which ultimately leads to an exciting new study compared to rare and precious base-metal photosensitizer.

Previous work in the group has focused on the synthesis and quantification of triplet excited state formation in the zinc(II) dipyrrin complexes shown in Figure 6.[60] Previous work by Alqahtani et al. showed that zinc(II) dipyrrin complex with iodine in THF solvent has a triplet quantum yield of 62% compared to zinc(II) dipyrrin complex without iodine that has triplet quantum yield of 29%, proving the author's hypothesis that the presence of iodine atoms would enhance the formation of triplet excited states.[60] This finding relates to this research because Alqahtani proved that iodine needs to be covalently bonded with the zinc(II) dipyrrin to have enhanced formation of triplet excited states (excellent photochemical properties of photosensitizer) compared to those without. Alqahtani also indicated that the increase in the quantum yield of the triplet state for zinc dipyrrin complex with iodine is not related to the increasing polarity of the solvent, the opposite is true for ZnDPY.[60] This research study will focus on photocatalysis using zinc(II) dipyrrin complexes as photosensitizers, illustrated in Figure 7.

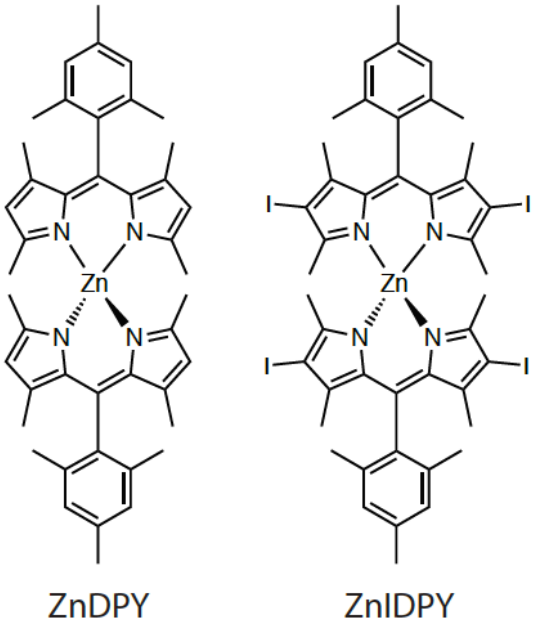

Figure 7. Target zinc(II) dipyrrin complexes for this research study.[60]

An appropriate catalyst must be paired with the photosensitizer so that the photocatalysis reaction can proceed. One property of an appropriate catalyst for this reaction is that it can be reduced by the photosensitizer. An example of such energetically appropriate catalysts are iron catalysts, like iron porphyrin complexes. Iron catalyst 5,10,15,20-tetrakis(pentafluorophenyl)-21H,23H-porphyriniron(III) chloride abbreviated [$FeF_{20}TPPCl$] fits the parameter according to Azacarate, wherein the catalyst must have a reduction potential less negative than the measured reduction potential of ZnDPY photosensitizer.[61] Iron porphyrin complexes are also found in the literature where these are used both in electrocatalytic[62,63] and photocatalytic CO_2 reduction processes.[13,64] Lastly, given its commercial availability and its appropriate energy, $FeF_{20}TPPCl$ was used as a catalyst. Hence, it can be reduced by the photosensitizers that is shown above in Figure 7.[65] The structure of the iron catalyst ($FeF_{20}TPPCl$) is shown in Figure 8.

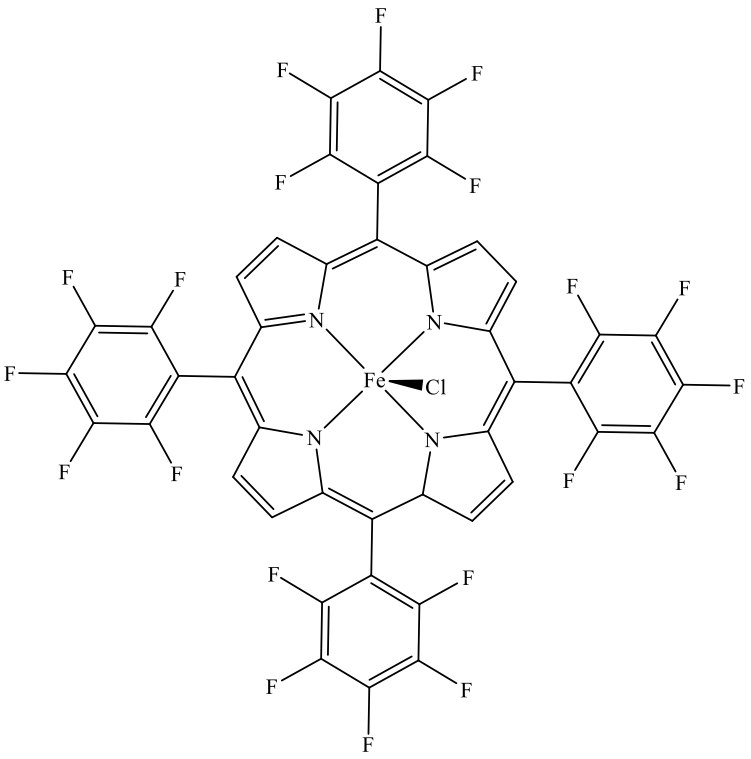

Figure 8. Chemical structure of 5,10,15,20-tetrakis(pentafluorophenyl)-21H,23H-porphyriniron(III) chloride ($FeF_{20}TPPCl$)

An energetically appropriate electron donor must have an oxidation potential capable of reducing the excited sensitizer. According to the calculated reduction potential of excited sensitizer molecule for ZnDPY and ZnIDPY, benzyl mercaptan shown in Figure 9 will be chosen as the electron donor in the experiment for testing the abilities of the photosensitizer.[66] Both potential energies of chosen iron catalyst and electron donor are energetically matched with both potentials of zinc(II) sensitizers, and as a result, reductive quenching pathway in Figure 4 will be the best fit for the reduction of carbon dioxide by photochemical system.

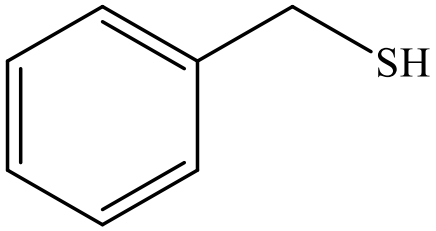

Figure 9. Chemical structure of benzyl mercaptan

In addition to photosensitizer, catalyst, and electron donor, a phenol, C_6H_5OH, is used in photocatalysis as an acid synergist. The acid synergist can stabilize the intermediate step of catalyst–CO2 carbenoid complex by hydrogen bonding.[45] Additionally, the presence of acid synergist is to increase the stability and catalytic efficiency of iron porphyrin catalyst based on the foundations of two-electron push-pull mechanism where $PFe(0)^{2-}$ pushes two electrons to the substrate CO_2 and the electron-poor acid synergist supports the adduct of one C-O bond.[45,67]

Excited State Electron Transfer and Photolysis with Zinc(II) Dipyrrin Sensitizers

A long-lived triplet excited state is not always an indication that a chromophore will be a suitable photosensitizer. Additionally, the triplet excited state must be able to undergo electron transfer. Figure 4[65] shows the reversible electrochemistry of the reductive quenching cycle for photocatalysis with a reductive catalyst.

As illustrated in Figure 4, the catalyst can oxidize the excited sensitizer, where the resulting oxidized sensitizer can be regenerated by an electron donor. Otherwise, the excited sensitizer can be reduced by an electron donor and then the reduced sensitizer can donate an electron to the catalyst so that the sensitizer can relax back to the ground state. For either mechanism, electron transfer is required for the excited state of the sensitizer. With this, the resulting oxidized or reduced sensitizer must be stable to experience a second electron transfer to regenerate the ground state sensitizer.

With this information, this study will aim to sensitize a photocatalytic reduction of carbon dioxide. The evaluation of the excited state electron transfer of zinc sensitizers is the first objective of this research study. The first step is to measure the electrochemical potentials of the ground state of the two zinc(II) complexes in Figure 7 using cyclic voltammetry. In the second step, the excited state redox potential of the two zinc(II) dipyrrin complexes can be estimated using the approach of Rehm-Weller equations.[68] The measured electrochemical potentials can then be used to match the sensitizers with an energetically appropriate catalyst and a sacrificial electron donor in the second part of the project. Lastly, this study requires performing photocatalytic experiment. Sensitizer, catalyst, and electron donor will be combined in a solution that is saturated with carbon dioxide and irradiated with visible light. After a set irradiation

period, the carbon monoxide that is formed by photocatalysis will be identified and quantified by gas chromatography.

Research Aim

The overall aim of this research project is to catalytically transform carbon dioxide into new sources of energy, making fossil fuels a more renewable energy option. There are many carbon dioxide reduction catalysts which incorporate abundant first-row transition metals, but a lack of earth abundant sensitizers. According to the previous work conducted by Alqahtani et al. the quantum yield of triplet state formation in ZnIDPY increased to 62% compared to ZnDPY with quantum yield of 29%.[60] The increase in quantum yield of triplet state formation for ZnIDPY was due to the addition of iodine that was responsible for enhanced ISC.[60] As a result, we hypothesize that both of zinc(II) dipyrrin sensitizers will be able to meet the requirements of an ideal photosensitizer to drive the photocatalysis of CO_2 reduction together with the chosen catalyst and electron donor. Additionally, we hypothesize that ZnIDPY sensitizer would form more CO to diffuse to headspace due to the enhanced of ISC compared to ZnDPY during photocatalysis.

The objectives of this research were accomplished in two steps. First, the electrochemical potentials of the two complexes ZnDPY and ZnIDPY were measured in polar solvents. These measured potentials were used to determine the excited state redox potentials of zinc(II) sensitizers. In the second step photocatalysis using a mixture of zinc(II) sensitizer, catalysts and electron donor was performed and the product formed was identified by gas chromatography.

CHAPTER 2: EXPERIMENTAL

Materials

Carbon dioxide (high purity) was purchased from AirGas. Iron catalyst, 5,10,15,20-tetrakis(pentafluorophenyl)-21H,23H-porphyriniron(III) chloride (≥95% HPLC purity) was purchased from Sigma Aldrich. Acetonitrile (HPLC grade), dichloromethane (certified ACS stabilized), tetrahydrofuran (HPLC grade), benzyl mercaptan (99% purity), ferrocene (99% purity), phenol crystalline (certified ACS +99% stabilized), tetrabutylammonium hexafluorophosphate (recrystallized and dried before use), and silver nitrate (certified ACS +99% purity metals basis) were purchased from Fisher Chemical. Both of photosensitizers Bis (1,3,7,9-tetramethyl-5-mesityldipyrrinato) zinc(II) complex [ZnDPY] and Bis (2,8-diiodo-1,3,7,9- tetramethyl-5-mesityldipyrrinato) zinc(II) [ZnIDPY] were synthesized in the lab by Norah Alqahtani. [65]

Methods

Cyclic Voltammetry (CV) Data Acquisition for Zinc(II) Photosensitizers

Cyclic voltammetry was performed using a Pine potentiostat WaveNow and a potential range of (±4.0 V). AfterMath software was used for the operation and data interpretation of the potentiostat. THF (HPLC grade) or DCM (HPLC grade) was used as the solvent with 0.1 M $TBAPF_6$ as the supporting electrolyte. For a water-free electrochemistry, non-aqueous referenced electrode (RE) was used. It consisted of a silver wire immersed in a solution contained 0.01 M $AgNO_3$ and 0.1 M tetrabutylammonium hexafluorophosphate ($TBAPF_6$) in HPLC grade acetonitrile (CH_3CN). A glassy carbon electrode was used as a working electrode (WE). Platinum wire was used as the counter electrode (CE). A schematic representation of the simple RE is shown in Figure 10.[69]

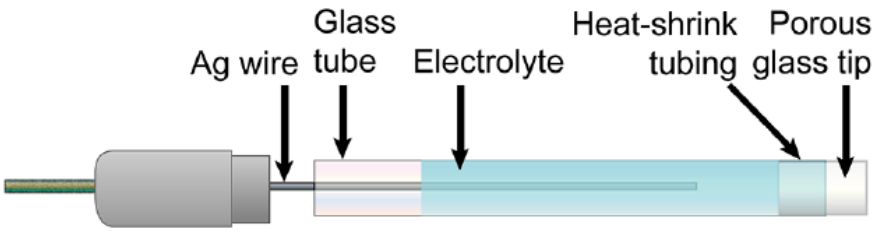

Figure 10. Simple non-aqueous reference electrode filled with reference solution is used in CV experiment. [69]. Reprinted with premission from Elgrishi, N.; Rountree, K. J.; McCarthy, B. D.; Rountree, E. S.; Eisenhart, T. T.; Dempsey, J. L. A Practical Beginner's Guide to Cyclic Voltammetry. J. Chem. Educ. **2018**, 95 (2), 197–206. https://doi.org/10.1021/acs.jchemed.7b00361. Copyright (2017) American Chemical Society

The electrolyte solution, 5 mL, was placed in a sealed vial, and nitrogen gas was bubbled in the solution for about 5 minutes to remove dissolved oxygen. The sealed vial and all other necessary components were placed inside a nitrogen filled glove bag. Inside the glove bag, the electrochemical cell was assembled. Electrochemical reversibility was established using CV and the reported redox potentials of zinc(II) sensitizers were determined relative to a ferrocenium/ferrocene (Fc^+/Fc) that was added to electrochemical cell as an internal standard. Redox potentials of ZnDPY was measured with THF solvent. Redox potentials of ZnIDPY was first performed with THF solvent and second with DCM. In both redox measurements of ZnIDPY, ferrocene was used as external standard due to overlaps of the analyte peak with ferrocene peak. A scan rate of 100 mV/s was used for all potential measurements.

Detection and Calibration Methods of Carbon Monoxide by GC

A SRI gas chromatography (310) instrument was used for the detection of carbon monoxide for the photocatalysis experiment. The GC is equipped with a thermal conductivity detector (TCD) and a 5A molecular sieve column. Over 60 injection trials, the best method for the identification and separation of CO peak was based on using helium as the carrier gas, a flow rate of 10 mL/min, oven temperature held at 60 °C and the TCD detector's temperature set at 100

°C. A Scott Mini-Mix gas cylinder contained 0.5% moles of homogenized gases of carbon monoxide, oxygen, carbon dioxide, and hydrogen in nitrogen gas was used for the calibration of the GC instrument. The retention time for CO peak was 5.40 minutes. Calibration curves for CO was determined by injecting 0.1-1.00 mL of the calibration gas. Injection of sample was performed using 1.00 mL disposable polypropylene syringe.

Photocatalysis Experiment Setup using ZDPY and ZnIDPY as Photosensitizer

A scintillation vial with a capacity of 24.144 mL was used to hold the reaction mixture of photocatalysis experiment. The total volume used for the reaction mixture in the reactor vial was 10 mL. The final concentrations after dilution to 10 mL THF are $3.5x10^{-6}$ M for ZnDPY/ZnIDPY, $2x10^{-6}$ M for iron catalyst, 0.36 M for electron donor, and 2 M for phenol. By optimizing the concentration of sensitizer only, these concentrations offer the maximum amount of CO that can be detected in headspace by GC. The final concentrations for both sensitizers were calculated based on the assumption of 99% absorption of visible light. Final concentrations for iron catalyst, electron donor, and phenol were chosen based on a study conducted by Bonin et. al. for the photochemical reduction of CO_2.[13] The reactor vial was sealed with a septa and threaded cap. Then, it was bubbled with CO_2 for 30 minutes. The reactor vial was irradiated by 300 W Xe arc lamp. The Xe arc lamp was running at 275 W. An optic filter was placed between the lamp and the reactor vial to block wavelengths below 455 nm. A glass water filter was placed between the optic filter and the reactor vial to absorb NIR and IR part of the lamp spectrum. The reactor vial was placed in a temperature-controlled water bath at 25 ^{o}C using ISOTEMP 4100 R20F. Figure 11 shows the photocatalysis experiment setup with its components.

The photocatalysis experiment was performed for about 65 hours when the amount of CO formed in headspace is slowing down. The headspace of the reactor vial was periodically sampled by withdrawing 1.00 mL using a syringe, which was injected directly into the GC. Three duplicated trials of photocatalysis experiment with each sensitizer were performed to check the reproducibility of CO produced in headspace under the same conditions. For each reaction mixture, two UV-Vis spectra were taken. The first UV-Vis spectra was taken immediately after preparing the reaction mixture and the second UV-Vis spectra was taken immediately after the photocatalysis experiment stopped.

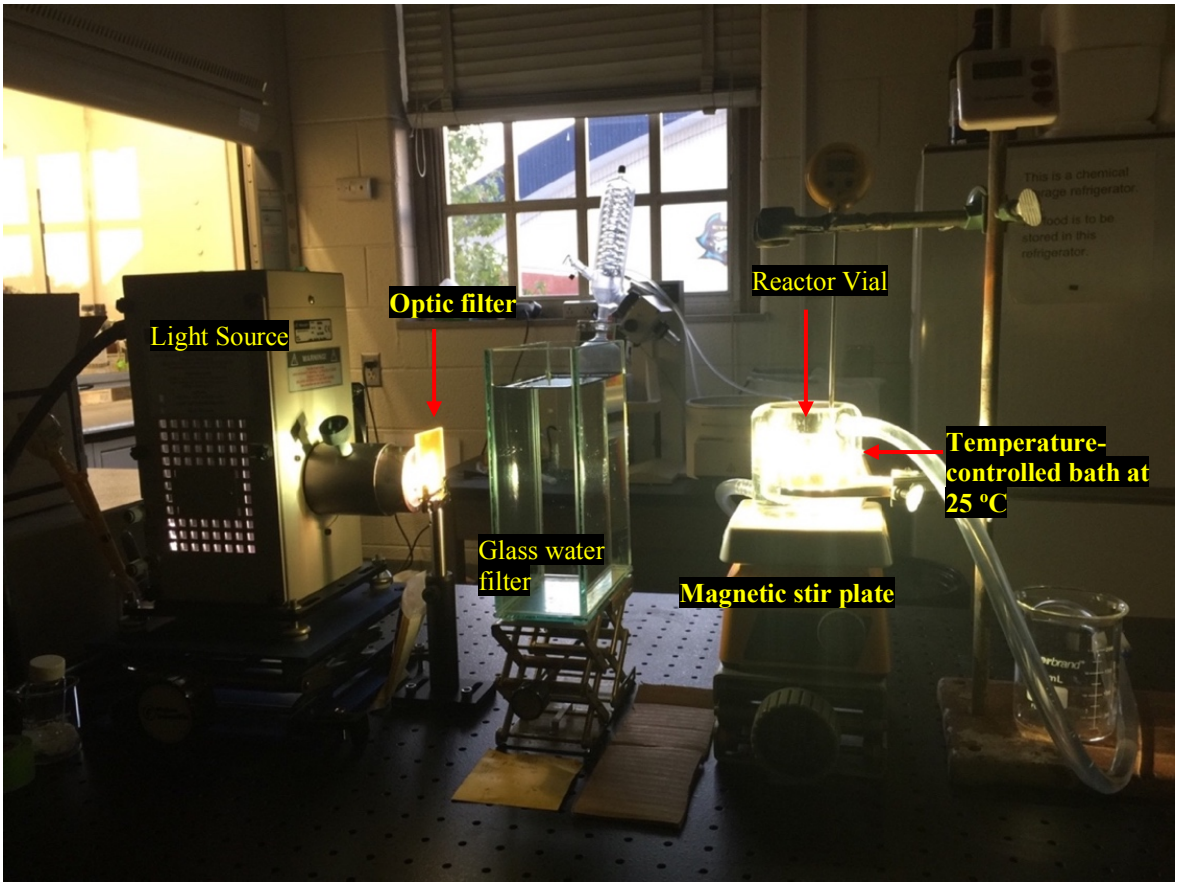

Figure 11. A picture shows the actual experimental components setup for photocatalysis reaction

Three different control experiments were performed to prove that the carbon monoxide product originated from the reduction of carbon dioxide. One control experiment was done by having the sealed reactor vial bubbled for 30 minutes with nitrogen gas instead of carbon dioxide gas. The second control experiment was done by blocking the visible light from reaching the reactor vial bubbled with carbon dioxide. The third control experiment was performed by having the headspace (HS) of reactor vial containing reaction mixture filled with calibration gas and blocking the light source from reaching the reactor vial.

Initial Rate of Product Formation of Carbon Monoxide by Photocatalysis

To compare how fast the carbon monoxide product was produced in the headspace by photocatalysis of the two different photosensitizers, the initial rate for each photocatalysis reaction associated with its specific sensitizer was estimated. The initial rate of reaction was estimated based on a plot of concentrations of carbon monoxide formed verses time. Generally, to calculate the rate of reaction using a plot, a tangent line can be drawn anywhere along the curve of CO formed vs. time. However, the tangent in this case was chosen to be drawn as soon as CO started to form in headspace. This will provide an appropriate measure of the initial rate of reaction. The gradient of the tangent line was used as a measure of initial rate of reaction. Equation (1) was used to calculate the rate of carbon monoxide formation using both photosensitizers.

Slope of tangent line = initial Rate = $\frac{\Delta[CO]}{\Delta t}$ (1)

CHAPTER 3: RESULTS AND DISCUSSION

Measuring Redox Potentials for Zinc(II) Dipyrrin Complexes Using CV

Cyclic voltammetry (CV) is a powerful technique used to investigate the electrochemical behavior (oxidation/reduction potentials, reversibility, etc.) of a redox-active species. Here, CV was used to measure the electrochemical potentials of the ground state for the two complexes ZnDPY and ZnIDPY. With these measured potentials, the excited state redox potentials for both sensitizers was determined using Rehm-Weller equations. To successfully drive the reduction of CO_2 by photochemical system, the redox potential values of both ground and excited state for zinc(II) sensitizers will be matched to energetically appropriate catalyst and electron donor.

In electrochemistry potential measurements, the presence of oxygen during potential measurement in open atmosphere causes a reversible one-electron reduction peak to form oxygen radical anion.[69] As a result, the presence of oxygen in an electrochemical experiment can alter the electrochemical response by overlapping with the analyte peaks.[69] To overcome the interference from the dissolved oxygen during electrochemical potential measurements, the prepared electrolyte solution was bubbled with nitrogen gas prior to taking every CV measurement. Additionally, each CV experiment was performed in a glove bag that was filled with nitrogen gas. Figure 12 represents CV scan for ZnDPY referenced to ferrocene that was added to cell as internal standard. The voltammogram of ZnDPY complex in Figure 12 showed two reversible reductions peaks potentials $(E_{1/2})_{red1}$ is -2.329 V and $(E_{1/2})_{red\ 2}$ is -2.671 and one reversible oxidation potential $(E_{1/2})_{ox}$ is 0.3892 V. In the study conducted by Tungulin et al. for zinc(II) Dipyrromethene CV scan, they have illustrated that both of oxidation and reduction potentials are assigned to the ligand.[58] With this information, the voltammogram of ZnDPY in Figure 12 shows the first referenced reduction value of ZnDPY is attributed to one-electron

reduction of π^*-orbital localized on the dipyrrin ligand. The second referenced reduction value is also attributed to the same process. The existence of two different waves for the same process can be assigned to Coloumbic repulsion and not to any difference in energy and/or electronic communication of the identical ligands.[70] The potential value of one referenced reversible oxidation for ZnDPY in Figure 12 is assigned to one-electron oxidation of the π-orbital of the ligand. Number of electrons (n) involved in this cyclic voltammogram is one and it was estimated based on a peak-to-peak difference of anodic and cathodic potentials that equal to theoretical value of 59mV/n.

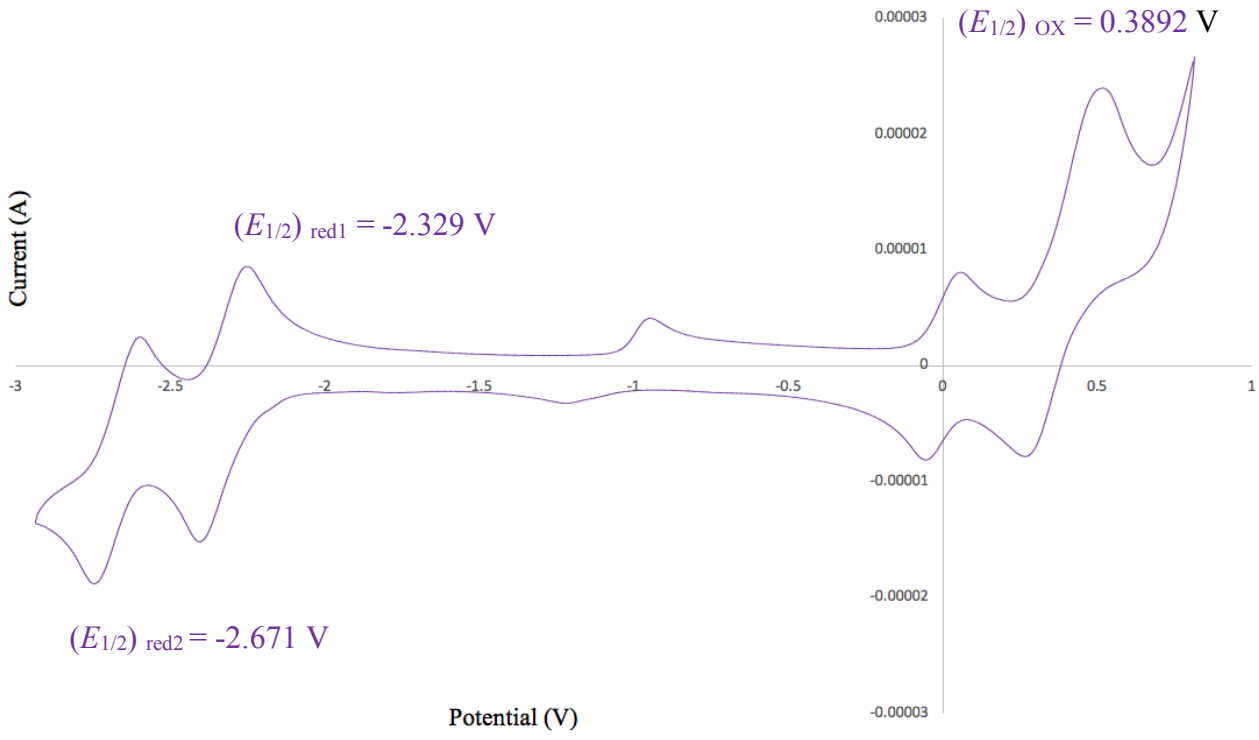

Figure 12. Cyclic voltammogram of ZnDPY showing both reduction potentials and one oxidation potential referenced to ferrocene in 0.1 M $TBAPF_6$ with THF solvent

For ZnIDPY photosensitizer, CV revealed two reduction potentials for ZnIDPY. The values of the first $(E_{1/2})_{red\ 1}$ and second $(E_{1/2})_{red\ 2}$ reductions potentials are -1.8901 V and -2.7271 V, respectively. Both reductions potentials were calculated with respect to ferrocene that was added as external standard. The voltammogram of the first reversible and second quasi-reversible reductions potentials for ZnIDPY in THF that were referenced to ferrocene are shown in Figures 13 and 14, respectively. Again, according to Tungulin at el. both reductions potentials of ZnIDPY in Figure 13 and 14 are assigned to one-electron reduction of π^*-orbital localized on the dipyrrin ligand.[58]

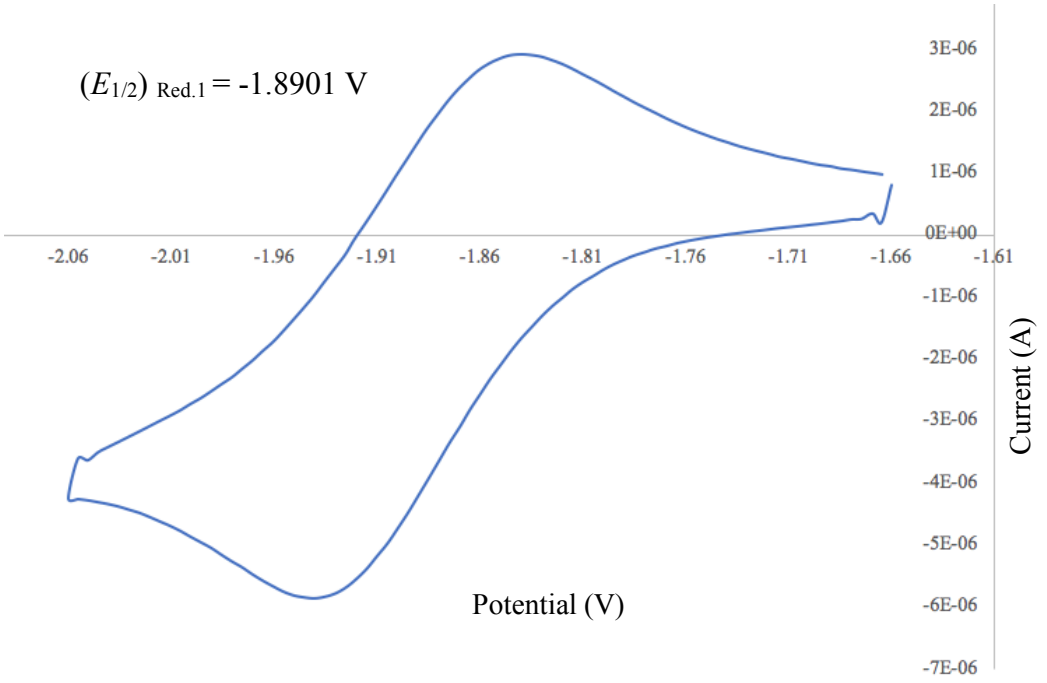

Figure 13. Voltammogram of ZnIDPY in 0.1 M $TBAPF_6$ electrolyte showing the first reduction potential referenced to ferrocene in THF solvent

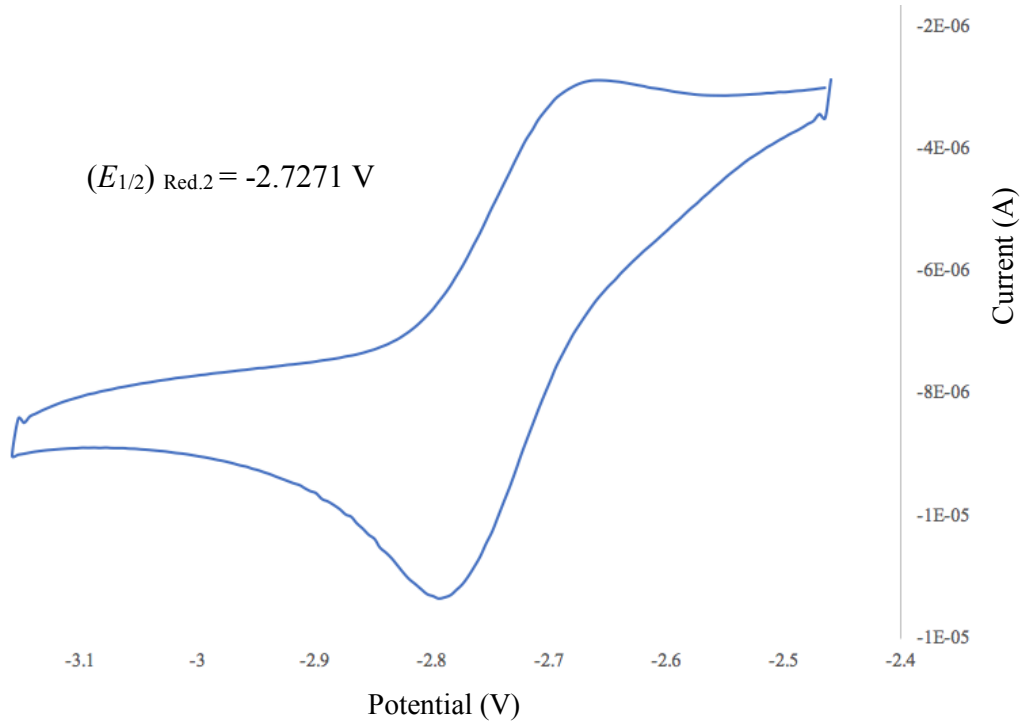

Figure 14. Voltammogram of ZnIDPY in 0.1 M $TBAPF_6$ electrolyte showing the second reduction potential referenced to ferrocene in THF solvent

In THF solvent, peaks potentials of both ferrocene and ZnIDPY are overlapping with each other's in the positive scan range of 0.1-1.0 V. As a result, the oxidation's peak potential for ZnIDPY complex was investigated in DCM solvent. Figure 15 represents oxidation peak potentials for ZnIDPY referenced to ferrocene in DCM solvent. The voltammogram in Figure 15 shows only two oxidations potentials for ZnIDPY complex between the scan range of 1 to 0.3 V. The first oxidation potential $(E_{1/2})_{OX1}$ has a value of 0.71059 V while the second oxidation potential $(E_{1/2})_{OX2}$ has a value of 0.49795 V. Both oxidation potentials for ZnIDPY were referenced to ferrocene that was added as external standard. Both oxidations potentials are assigned to the ligand due to one-electron oxidation of π-orbital localized on the dipyrrin ligand.

The redox potential values of ground state for both zinc(II) sensitizers were obtained experimentally using CV, where the collected data are shown in Table 2. The redox potentials of excited state of ZnDPY and ZnIDPY sensitizers were calculated using the redox potential values of the ground states. Rehm-Weller Equations 2[68] and 3[68] below are used for this purpose.

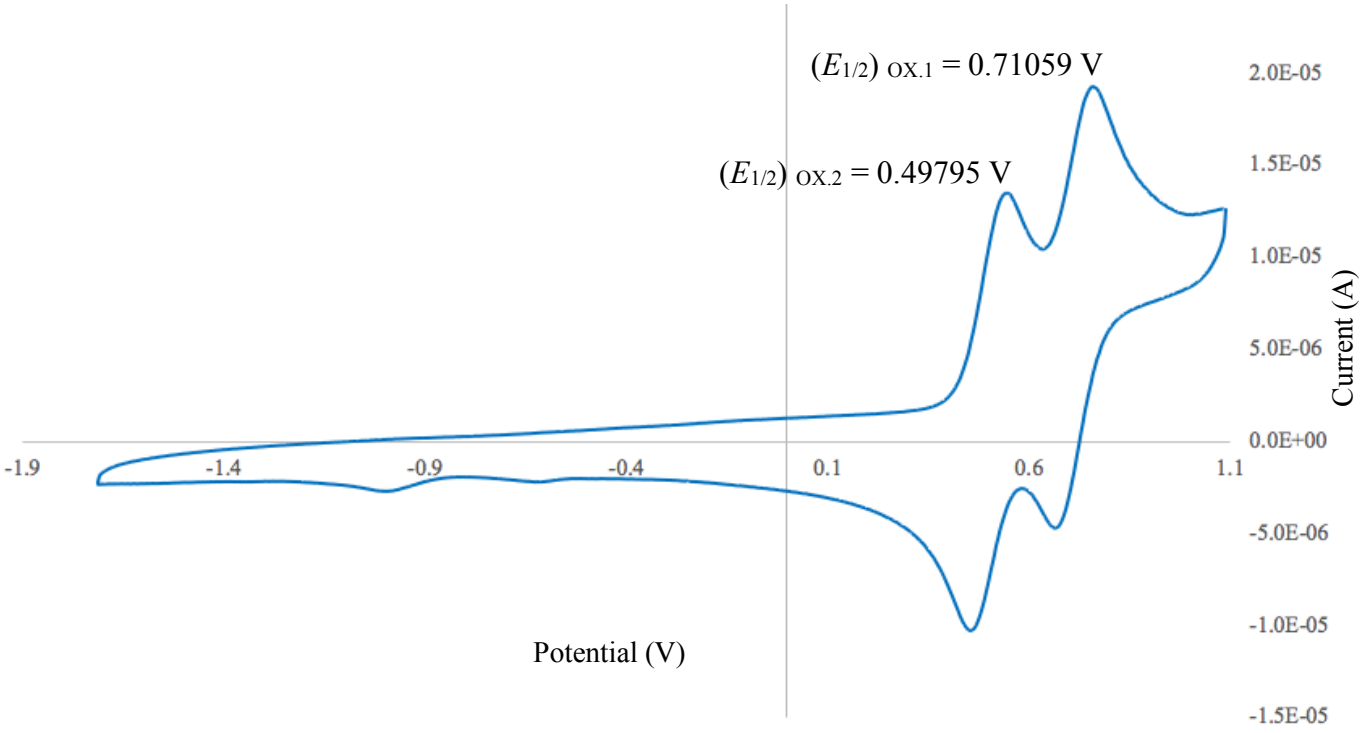

Figure 15. Voltammogram of ZnIDPY complex referenced to ferrocene in DCM solvent and 0.1 M $TBAPF_6$ electrolyte and it is showing two oxidations potentials

Table 2. Redox Potential Values of the Ground State of Zinc(II) Dipyrrin Complexes Referenced to Ferrocene, Measured by Cyclic Voltammetry

Sample	Solvent	$(E_{1/2})_{\text{Ox. 1}}$	$(E_{1/2})_{\text{Ox. 2}}$	$(E_{1/2})_{\text{Red. 1}}$	$(E_{1/2})_{\text{Red. 2}}$
ZnDPY	0.1 M $TBAPF_6$ with THF	0.3892 V	NA	-2.329 V	-2.671 V
ZnIDPY	0.1 M $TBAPF_6$ with THF	NA	NA	-1.8959 V	-2.7271 V
	0.1 M $TBAPF_6$ with DCM	0.49795 V	0.71059 V	NA	NA

Calculation for the Excited State Redox Potential for Zinc(II) Dipyrrin Complexes

Both Equations 2[68] and 3[68] and the calculated values of the redox potentials of the ground state of both zinc(II) sensitizer were used to calculate the redox potentials of the orbitals in the excited state of ZnDPY and ZnIDPY. The term E_T represents energy of the triplet state for ZnDPY and ZnIDPY. The value of E_T for ZnIDPY was based on the emission spectra of ZnIDPY recorded at 77 K in frozen 2-Me THF (red) as shown in Figure 16.[60] The value of E_T for ZnDPY was obtained from literature.[56]

$$\boldsymbol{E_{Ox}^{oZnDPY,\ ZnIDPY*} = E_{Ox}^{oZnDPY,\ ZnIDPY} - E_T} \quad (2)$$

$$\boldsymbol{E_{Red}^{oZnDPY,\ ZnIDPY*} = E_{Red}^{oZnDPY,\ ZnIDPY} + E_T} \quad (3)$$

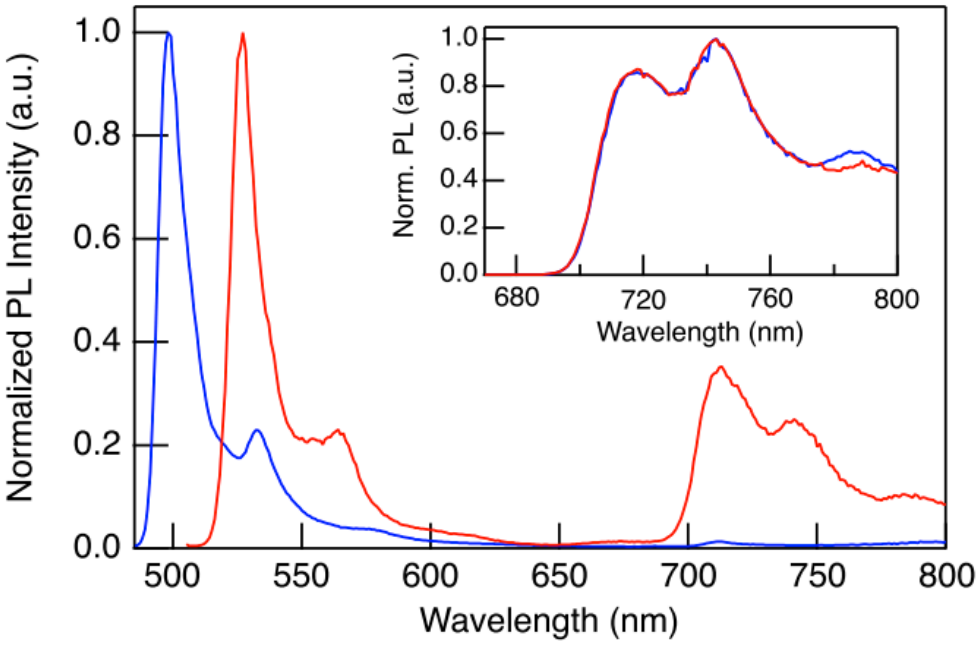

Figure 16. Normalized low temperature emission spectra for ZnDPY (blue) and ZnIDPY (red) recorded at 77 K in frozen 2-Me THF solution. [60] Reprinted with permission from Alqahtani, N. Z.; Blevins, T. G.; McCusker, C. E. Quantifying Triplet State Formation in Zinc Dipyrrin Complexes. *J. Phys. Chem. A* **2019**. https://doi.org/10.1021/acs.jpca.9b08682. Copyright (2019) American Chemical Society

The potential values of the ground state shown in Table 2 and the calculated potential values of the excited states were converted to V vs. SCE.[71] The conversion $E^{\circ}_{1/2}$ (Fc/Fc^{+}) = +0.547 V vs. SCE in THF solvent was used to produce an energy diagram shown in Figure 17. In order to perform photocatalysis experiment, a catalyst and sacrificial donor were chosen for each sensitizer (ZnDPY and ZnIDPY).

For a successful photocatalysis experiment, the electrochemical potential for both sensitizers must match with an energetically appropriate catalyst and sacrificial electron donor. A sacrificial donor and a catalyst were chosen for both photosensitizers. Both the chosen catalyst and sacrificial donor along with sensitizers have undergone reductive quenching cycle to transform the available carbon dioxide in the latter to carbon monoxide.

The catalyst in the excited state was first reduced and then oxidized to return to the ground state. Iron catalyst ($FeF_{20}TPPCl$)[72] and sacrificial electron donor (Benz-s)[66] were chosen for both sensitizers. The iron catalyst used in the experiment was commercially available. It was used for both sensitizers to perform photocatalysis experiment. Both potential energies for catalysts and electron donor were included into the orbital's energy diagram illustrated in Figure 17. This was done for a possible reductive quenching cycle to successfully drive the photochemical reduction of carbon dioxide using visible light.

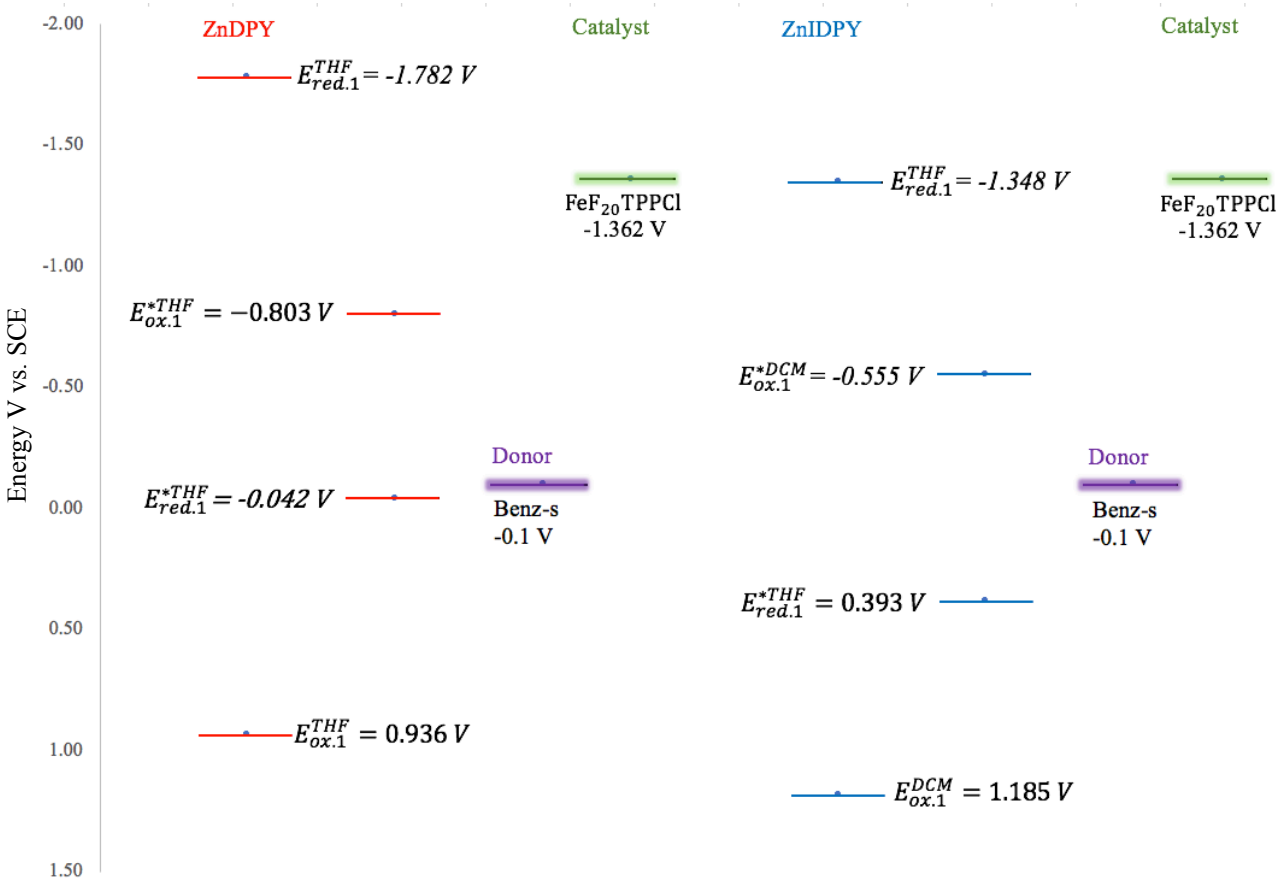

Figure 17. Energy diagram shows the energy of the chosen catalysts and sacrificial donor for ZnDPY and ZnIDPY sensitizers

Calibration Curve of Carbon Monoxide

The carbon monoxide sample used for the calibration of GC instrument contained a mixture of 14 liters of gas pressurized at 17 bar and 21°C to approximately a 2 liter cylinder. The cylinder contained 0.5% moles of homogenized gases of carbon monoxide, oxygen, carbon dioxide, and hydrogen in nitrogen gas. A capacity of 1.00 mL disposable polypropylene syringe was used for sample injection. Known volumes that ranged from 0.1 mL to 1.00 mL of the same sample that described above was injected directly into GC to produce a calibration curve of CO shown in Figure 18.

At this point, the calibration curve of carbon monoxide was used to determine both the limit of detection (LOD) and limit of quantification (LOQ). Equations 4[73] and 5[73] were used to calculate the LOD and LOQ, respectively. A signal-to-noise ration of 3:1 and 10:1 are considered acceptable limits for estimating limit of detection and limit of quantification, respectively. In the equations, *m* represents the slope of the calibration curve with a value of 1072.5 peak area/µmole CO. Meanwhile, *S* represents the standard deviation (1.287) of the signal. The calculated value of LOD is 0.0036 µmole and LOQ is 0.012 µmole.

$$\mathrm{LOD} = 3S/m \tag{4}$$

$$\mathrm{LOQ} = 10S/m \tag{5}$$

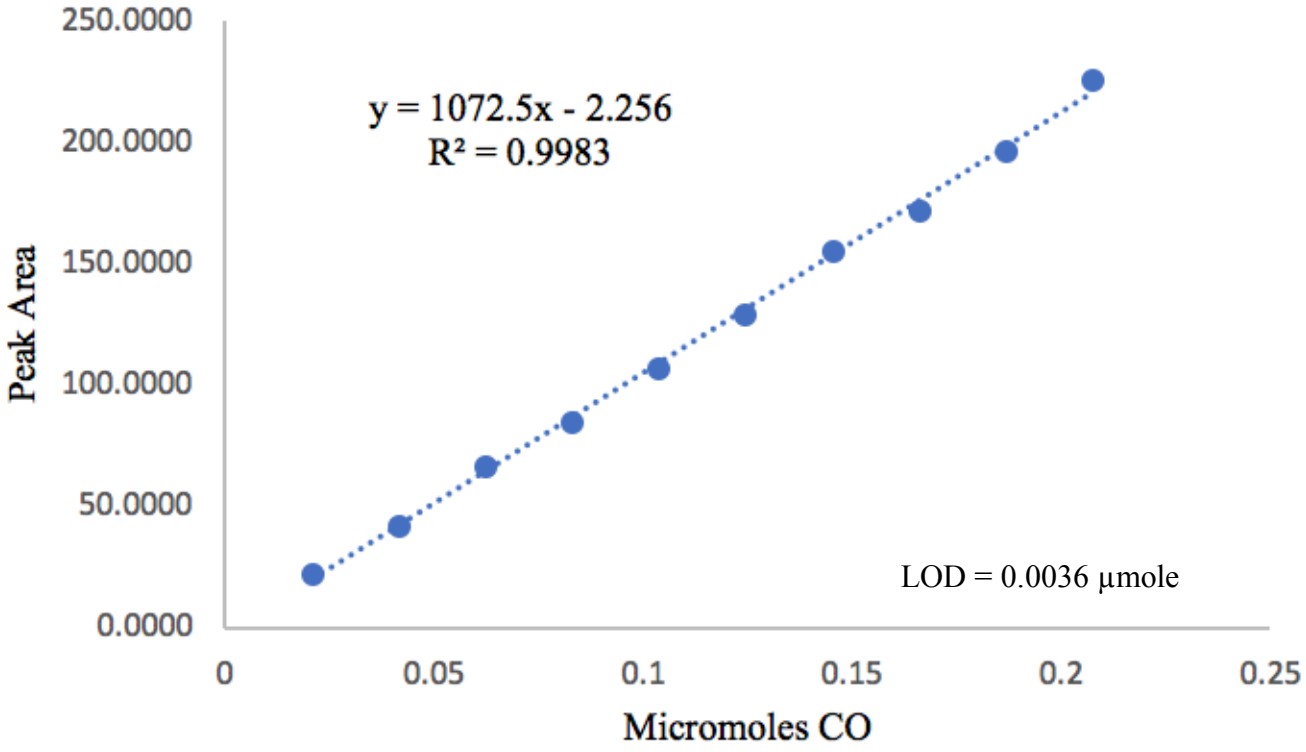

Figure 18. Calibration curve of carbon monoxide. Calibration gas is contained 0.5% moles of homogenized gases of CO, O_2, CO_2, and H_2 in N_2 gas pressurized at 17 bar in 2 liters cylinder. Dash line represents a direct proportional response between GC and detected amount of CO. LOD represents lowest amount of CO can be detected within a specified analytical method

UV-Vis Absorption Spectra for Catalyst and both Photosensitizers

The UV-Vis absorption spectra for iron catalyst and both photosensitizers were obtained and are shown in Figure 19. The maximum absorption wavelength for π to π* transition for inactive iron catalyst was found to be 412 nm, and the π to π* transition for ZnDPY and ZnIDPY photosensitizers were determined to be 490 nm and 513 nm, respectively. The inactive iron catalyst has a chlorine attached to the central metal Fe(III)-Cl as shown in Figure 8 above. During photocatalysis, chlorine is dissociated and allowing Fe(III)F_{20}TPP to be reduced by a photosensitizer to its active state Fe(0)F_{20}TPP. The purpose of the obtained absorption spectra for catalyst and both sensitizers is to ensure that most of the light in the visible region during the photocatalysis experiment is being absorbed by the photosensitizer and not by the iron catalyst.

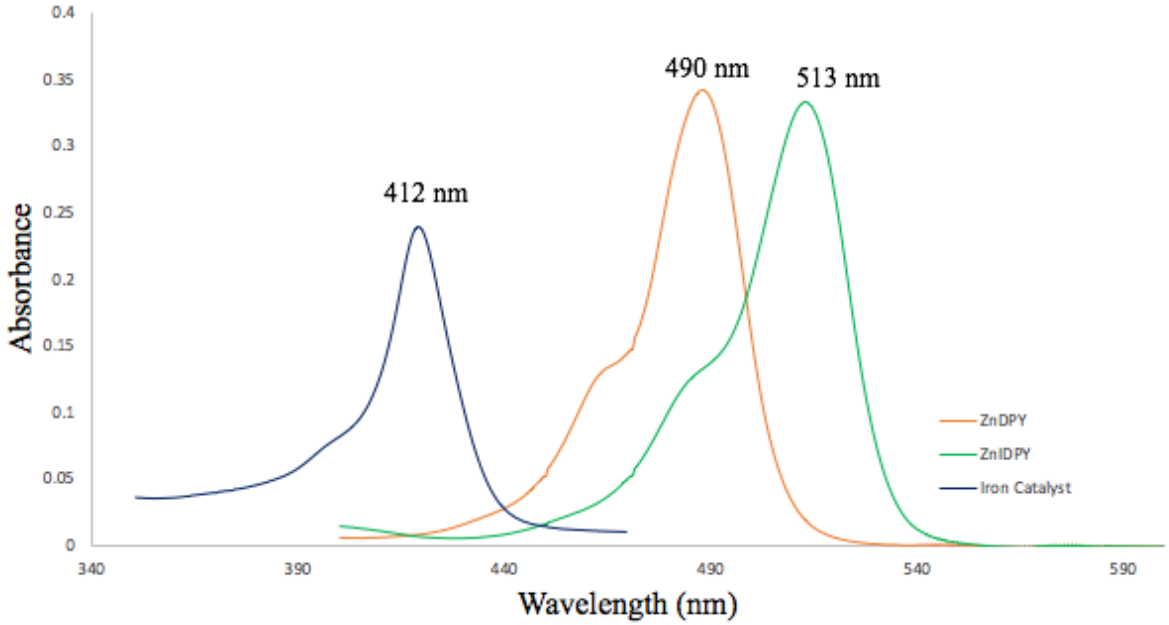

Figure 19. UV-Visible absorption spectra for iron catalyst and both photosensitizers in THF solvent. Concentration of iron catalyst is $2x10^{-6}$ M and $3.5x10^{-6}$ M for both photosensitizers

Data Analysis for Carbon Dioxide Reduction using ZnDPY as Photosensitizer

The data analysis of photocatalysis experiment setup for carbon dioxide reduction using $3.5x10^{-6}$ M ZnDPY, $2x10^{-6}$ M iron catalyst, 0.36 M electron donor, and 2 M phenol in 10 mL THF. The reactor vial was sealed and then it was bubbled with carbon dioxide for 30 minutes. Then, it was irradiated for 65 hours using Xe arc lamp and optic filter. Eight samples were done by drawing 1.00 mL from the headspace of the reactor vial and injected directly into the GC. The peak area of the detected CO was used to calculate micromoles of CO in 1.00 mL of the injected sample, utilizing the equation of the calibration curve. Table 3 shows the amount of CO generated in the headspace for 65 hours. The amount of CO in headspace for the first trial for injections 1-8 are calculated based on Equation (6) of the calibration line and based on vial's headspace volume of 14.144 mL.

$$y = 1072.5X - 2.25 \quad (6)$$

As mentioned in the experimental and method chapter, the photocatalysis experiment for the reduction of carbon dioxide was required to be replicated for three more trials. This was done to ensure that the same amount of carbon monoxide can be generated in the headspace of the reactor vial over the same amount of time. The data collected for the average total amount of CO produced in the headspace of the three trials are shown in Table 3. The collected data in Table 3 clearly shows an increase in the production of carbon monoxide in the head space over time. These data were averaged and plotted against average irradiation time as shown in Figure 20. The TON was calculated using Equation 7 and illustrated in Table 3.

$$\text{TON} = \frac{\text{Total µmole of CO in headspace for each injection point}}{\text{µmole of catalyst in solution}} \quad (7)$$

Table 3. Average Amount of Carbon Monoxide Generated in Headspace Over Time for the Three Trials using ZnDPY PS

Injection #	Avg. Hours	Avg. Total µmole CO in headspace	STD	TON of CO formation	STD
1	2	0.0349	± 0.0094	1.7	± 0.4
2	5	0.0565	± 0.0013	2.8	± 0.1
3	11	0.0687	± 0.0015	3.4	± 0.2
4	20	0.0878	± 0.0042	4.3	± 0.1
5	26	0.1038	± 0.0057	5.1	± 0.1
6	44	0.1181	± 0.0061	5.9	± 0.3
7	52	0.1383	± 0.0133	6.9	± 0.5
8	65	0.1464	± 0.0097	7.3	± 0.1

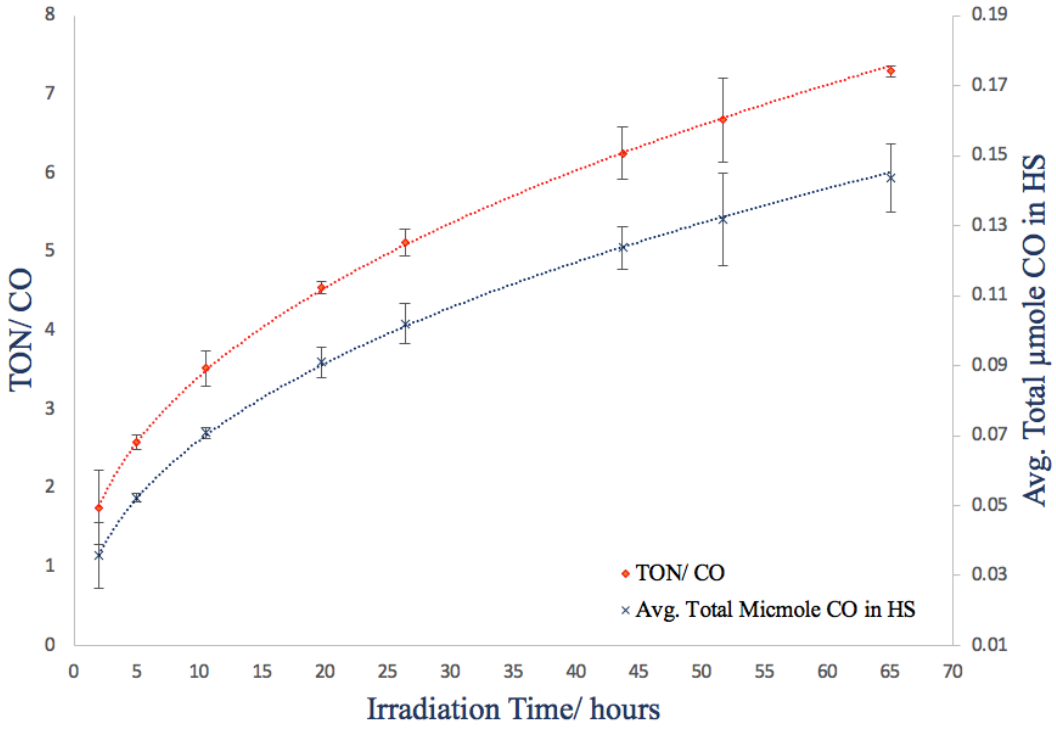

Figure 20. Average amount of CO produced in the headspace using ZnDPY PS for a 65-hour irradiation is shown on the right-side axis. Meanwhile, TON of CO is shown on the left- side axis. The dotted lines represent a smooth increase of CO in HS overtime. Error bars represents the three duplicated trials

Figure 20 shows the amount of carbon monoxide generated is reproducible over time. It also shows that the rate of carbon monoxide produced in the headspace started to decrease between 55 and 65 hours. The variation (represented by error bars) may be due to a few factors. First, is the time related to sampling. Second is the difficulty of weighing 1.0 mg and 1.5 mg for limited amount available of PS and catalyst, respectively. This might lead to variation in the concentration of each sample. The third factor is related to sample injection slow or fast injection leads to peak broadening and/or poor resolution. The standard deviation for each individual injection point is shown in the same figure. The calculated values for turnover number (TON) of carbon monoxide formation over time are listed in Table 3 and plotted in Figure 20. The TON of carbon monoxide formation exceeded 7.0 for a total irradiation time of 65 hours. This value is

much lower compared to a study conducted by Bonin that showed TON of up to 140 for the reaction mixture containing the same type of iron catalyst (FeTPP) coupled with the precious metal-based photosensitizer $Ir(ppy)_3$.[13] Rare metal-based catalyst such Ru and Re coupled with rare and expensive metal sensitizers (e.g. Ir and Ru) are reported with TON of 98,000.[38,74]

Data Analysis for Carbon Dioxide Reduction using ZnIDPY as Photosensitizer

Experimentally, photocatalysis of carbon dioxide reduction was performed with ZnIDPY photosensitizer in the same way as performed with ZnDPY. Data analysis of carbon monoxide generated over time in the headspace by photocatalytic system were collected. These were analyzed and calculated in the same way as ZnDPY sensitizer.

Table 4 shows the average total amount of CO generated in the headspace for the three replicated trials. The Table shows these values along with the TON of carbon monoxide formation by photocatalysis system. A plot of both the average total amount of carbon monoxide in headspace over time and TON are shown in Figure 21. The standard deviation for each individual injection point in Figure 21 was also calculated, which are shown in Table 4. The associated error bar is shown in the same plot. Figure 21 clearly shows reproducible trends for the increase in the amount of carbon monoxide produced in the headspace over time by photocatalytic reduction of carbon dioxide. For 83 hours of photocatalysis, the maximum value of TON was calculated 16. Figure 21 also shows that the amount of carbon monoxide in the headspace started to show a maintained level between 70 and 83 hours.

Table 4. Average Amount of Carbon Monoxide Generated in the Headspace for Approximately 83 Hours of Irradiation Time of the Three Replicated Trials using ZnIDPY PS

Injection #	Avg. Hours	Avg. Total µmole CO in headspace	STD	TON of CO formation	STD
1	2.3	0.0562	± 0.0031	2.8	± 0.1
2	6	0.1008	± 0.0076	5.0	± 0.3
3	12.3	0.1375	± 0.0199	6.8	± 1.1
4	22.3	0.1604	± 0.0188	8.0	± 0.6
5	27.3	0.1914	± 0.0239	9.5	± 0.8
6	35.8	0.2264	± 0.0168	11.3	± 0.6
7	46.5	0.2688	± 0.0044	13.4	± 0.1
8	54.0	0.2951	± 0.0120	14.7	± 0.1
9	70.5	0.3147	± 0.0083	15.7	± 0.3
10	83.5	0.3284	± 0.0061	16.4	± 0.3

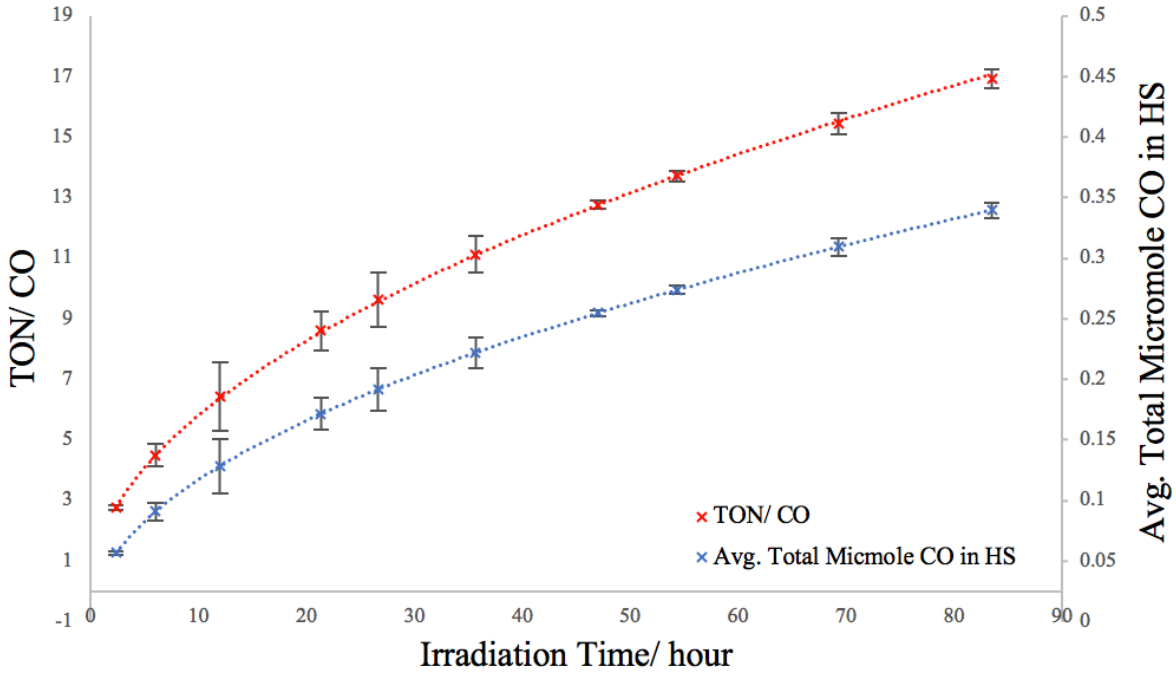

Figure 21. Average total amount of CO produced in the headspace using ZnIDPY PS for an 83-hour irradiation time is shown on the right-side axis. TON (red dots) of CO formation, which are exceeds 16, is shown on the left-side axis. The dotted lines represent a smooth increase of CO in HS overtime. Error bars represents the three duplicated trials

UV-Vis Absorption Spectra for Photocatalysis Reaction Mixture

UV-Vis absorption spectra of the reaction mixture in Figure 22 was obtained before photocatalysis experiment and immediately after stopping the experiment. The reaction mixture contains all experimental components including electron donor. However, Figure 22 is only showing the UV-Vis absorption region of interest for both the catalyst and sensitizer. Before photocatalysis, the inactive catalyst PFe(III) has chemical formula $FeF_{20}TPPCl$ with an absorption of 420 nm. Due to the many different oxidation states available after photocatalysis for iron catalyst (e.ge Fe^{II}, Fe^{I}, Fe^{0}, and Fe^{II}-CO), it's difficult to assign an absorption bond to only one of several existing oxidation states of the iron catalyst due to the overlapping of the absorptions spectra for all available oxidations states of iron catalyst in the region of approximately 400-420 nm.[10] So, the absorption at 422 nm in Figure 22 represents one of the available oxidation states of iron catalyst.

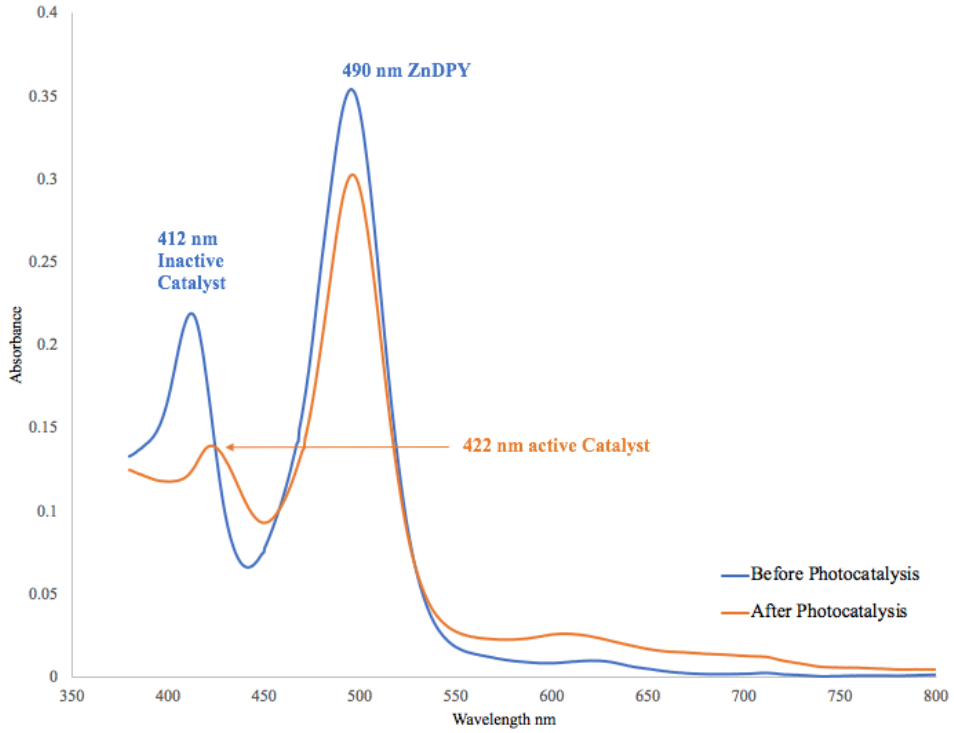

Figure 22. UV-Vis spectra for the reactor solution mixture before (blue) and after (orange) the photocatalysis. The photocatalysis experiment was performed for 65 hours

The sensitizer ZnDPY still has the same wavelength of maximum absorbance, 490 nm. However, the absorption has decreased because some of the excited sensitizer complexes are not able to regenerate over several cycles of oxidation and reduction and decomposes. UV-Vis absorption spectra before and after photocatalysis for a reaction mixture contained ZnIDPY coupled with iron catalyst, electron donor, and phenol is shown in Figure 23. After 83 hours of photocatalysis experiment, ZnIDPY decomposes much more compared to ZnDPY.

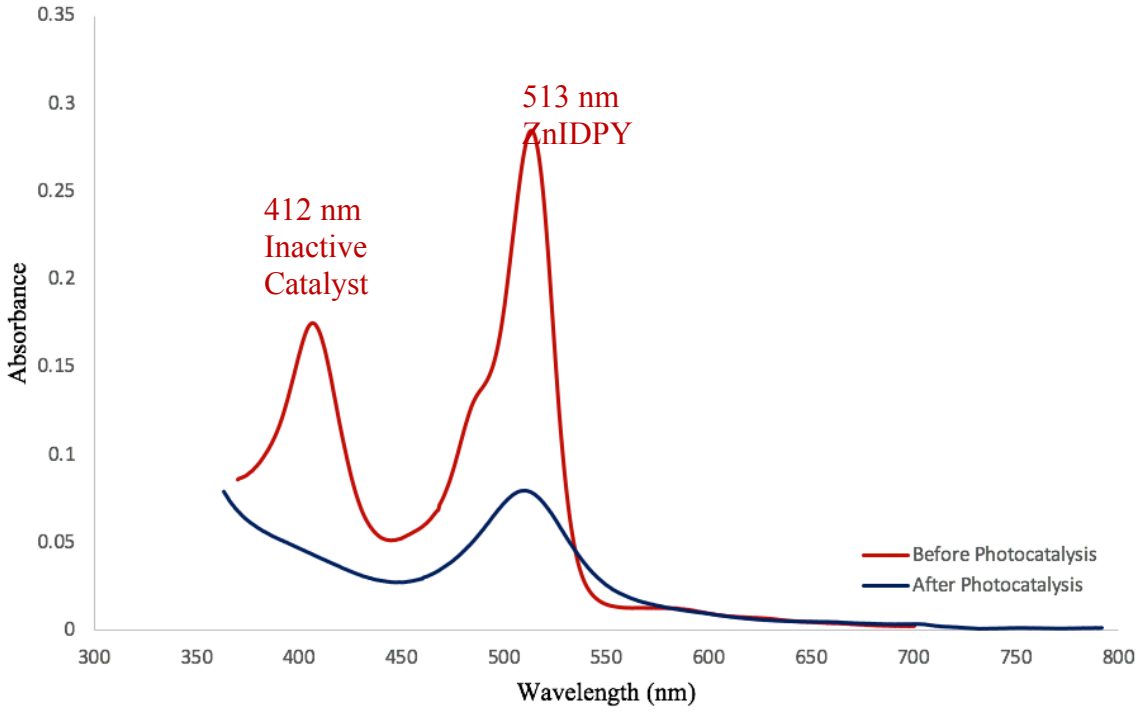

Figure 23. UV-Vis spectra for the reactor solution mixture before (red) and after (blue) the photocatalysis. The photocatalysis experiment was performed for 83 hours

Rate of Carbon Monoxide Produced by Photocatalysis using ZnDPY and ZnIDPY Sensitizer

The concentration of average total carbon monoxide produced in headspace for each injection was calculated using Table 3 for ZnDPY and Table 4 for ZnIDPY. The volume of headspace is 14.14 mL. A plot of concentration of carbon monoxide formed with respect to time for both photosensitizers is shown in Figure 24. From the plot, the slope related to reaction rate of ZnIDPY is steeper compared to that of ZnDPY. As a result, there is about 47% more of CO produced in headspace for photocatalysis reaction involving ZnIDPY sensitizer than ZnDPY. The initial rate of reaction for both photosensitizers was estimated using the slope of tangent line and Equation (1).

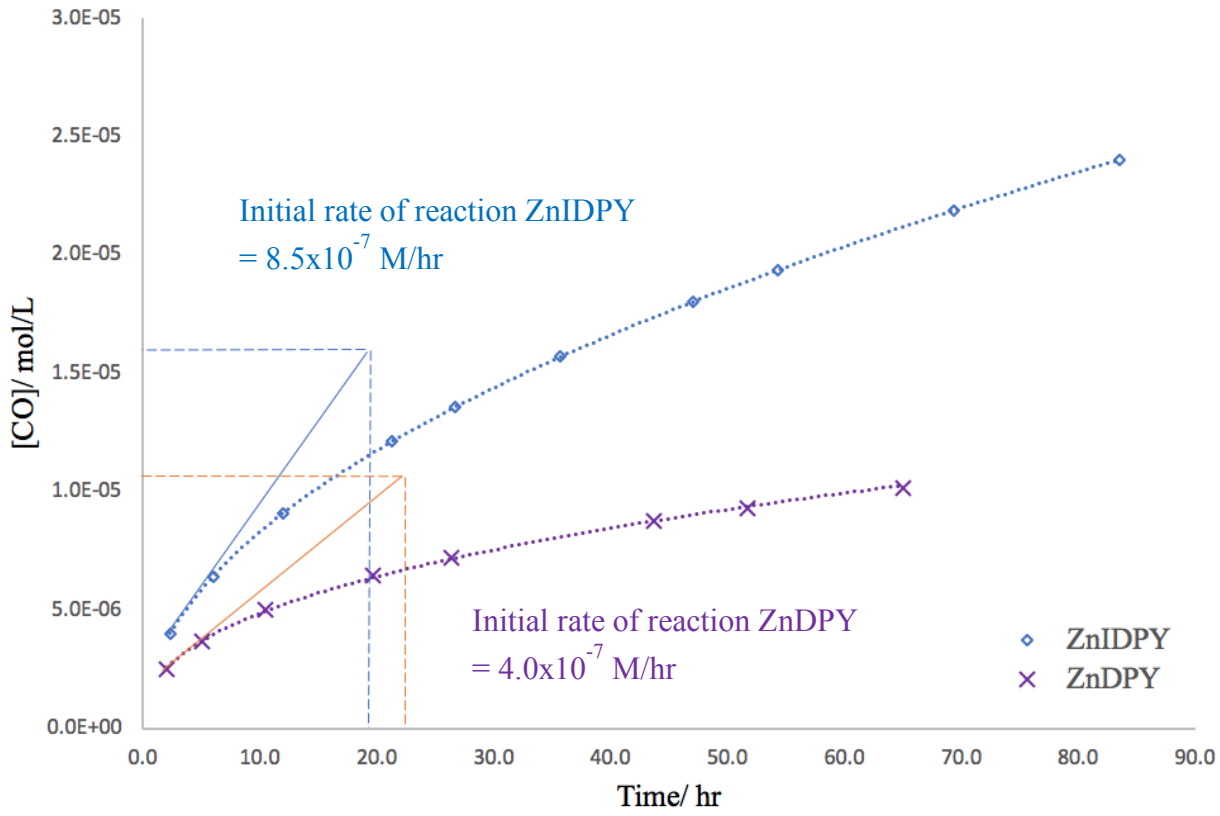

Figure 24. Reaction rate for the formation of CO by photocatalytic system for three duplicated trials with ZnDPY and ZnIDPY sensitizers

Photocatalysis Control Experiment

Two different control experiments were performed for both sensitizers (ZnDPY and ZnIDPY). For each sensitizer, one control experiment was done by having the reactor vial contain the reaction mixture bubbled with N_2 gas and irradiated with light source. The second control experiment was done by blocking the light source from reaching the reactor vial that contained the reaction mixture bubbled with CO_2. In the third control experiment, the headspace of a reactor vial containing the reaction mixture was filled with calibration gas to determine if CO is soluble in the solution. The light source was blocked from reaching the reactor vial. The headspace of reactor vial for the first and second control experiments were analyzed by GC for CO. Briefly, both control experiments showed no CO produced in the headspace. Analysis of the headspace for the third control experiment shows no CO diffused to the reaction mixture. These control experiments support that CO produced is due to photoreduction of CO_2. Also, the reaction rate is accurately measured by monitoring the amount of CO in the headspace.

CHAPTER 4: CONCLUSIONS

Experimental study and data analysis revealed that a new class of first-row transition metal zinc(II) dipyrrin photosensitizers were able to successfully drive a photocatalytic reduction system to convert the carbon dioxide into a highly stable product of carbon monoxide. The study of both sensitizers was accomplished in two steps. The first step to accomplish this study was by measuring the electrochemical potential of the orbitals in the ground and excited states of the two zinc(II) dipyrrin sensitizers. This was measured by cyclic voltammetry and was used to match them with an energetically appropriate catalyst ($FeF_{20}TPPCl$) from the first-row transition metals and an electron donor (Benz-s).

The second step was photocatalysis experiments performed using a mixture containing zinc(II) sensitizer, iron catalyst, and electron donor to reduce CO_2. This reaction mixture was irradiated with visible wavelength light in the presence of carbon dioxide. Carbon monoxide, the photocatalysis product, was identified and quantified by gas chromatography over time. The first set of photocatalysis experiments were performed using ZnDPY photosensitizer. Data analysis shows that the amount of carbon monoxide produced in the headspace by photocatalytic system increases over time during the total run time of 65 hours. The maximum TON obtained was 7.3 for the formation of carbon monoxide in headspace. This value is comparable to TON of 5-60 with same type of catalyst but coupled with rare and expensive sensitizer.[13]

On the other hand, the second set of photocatalysis experiments were performed using ZnIDPY photosensitizer. Data analysis also shows an increase in the amount of carbon monoxide during the total run time of 83 hours. The maximum TON obtained was 16.4 for the formation of carbon monoxide in headspace. Again, this value is still comparable to 5-60 TON using the same type of catalyst but coupled with rare and expensive sensitizer. There is about 47% more carbon

monoxide generated in the headspace over time using ZnIDPY photosensitizer in contrast to ZnDPY under the same experimental conditions as possible. These results are in agreements with first hypothesis for having first-row transition metal zinc(II) dipyrrin as a satisfactory photosensitizer. Also, the result comes with agreements with the second hypothesis for having more CO produced in headspace using ZnIDPY sensitizer compare to ZnDPY. Finally, the estimated initial rate of product formation by photocatalysis using ZnIDPY photosensitizer is faster than the initial rate estimated using ZnDPY photosensitizer.

REFERENCES

(1) Beller, M.; Junge, H.; Ludwig, R. Catalysis Science & Technology. **2015**. https://doi.org/10.1039/C5CY01129A

(2) Le Quéré, C.; Raupach, M. R.; Canadell, J. G.; Marland, G.; Bopp, L.; Ciais, P.; Conway, T. J.; Doney, S. C.; Feely, R. A.; Foster, P.; et al. Trends in the Sources and Sinks of Carbon Dioxide. *Nat. Geosci.* **2009**, *2* (12), 831–836. https://doi.org/10.1038/ngeo689

(3) Arnita Wuri, M.; Pertiwiningrum, A.; Budiarto, R.; Agus Dwi Koranto, C. Characterization of Natural Zeolite and Chicken Manure Derived Biochar for Carbon Dioxide Adsorption in Biogas. *E3S Web Conf.* **2018**, *43*, 2–5. https://doi.org/10.1051/e3sconf/20184301008

(4) Plasseraud, L. Carbon Dioxide as Chemical Feedstock. Edited by Michele Aresta. *ChemSusChem* **2010**, *3* (5), 631–632. https://doi.org/10.1002/cssc.201000097

(5) Laboratory, L. L. N. Estimated U.S. Energy Consumption in 2018 https://www.llnl.gov/news/us-energy-use-rises-highest-level-ever.

(6) Morris, A. J.; Meyer, G. J.; Fujita, E. Molecular Approaches to the Photocatalytic Reduction of Carbon Dioxide for Solar Fuels. *Acc. Chem. Res.* **2009**, *42* (12), 1983–1994. https://doi.org/10.1021/ar9001679

(7) Cokoja, M.; Bruckmeier, C.; Rieger, B.; Herrmann, W. A.; Kühn, F. E. Transformation of Carbon Dioxide with Homogeneous Transition-Metal Catalysts: A Molecular Solution to a Global Challenge? *Angew. Chemie - Int. Ed.* **2011**, *50* (37), 8510–8537. https://doi.org/10.1002/anie.201102010

(8) Kumar, B.; Llorente, M.; Froehlich, J.; Dang, T.; Sathrum, A.; Kubiak, C. P. Photochemical and Photoelectrochemical Reduction of CO 2 . *Annu. Rev. Phys. Chem.*

2012, *63* (1), 541–569. https://doi.org/10.1146/annurev-physchem-032511-143759

(9) Reithmeier, R.; Bruckmeier, C.; Rieger, B. Conversion of CO_2 via Visible Light Promoted Homogeneous Redox Catalysis. *Catalysts* **2012**, *2* (4), 544–571. https://doi.org/10.3390/catal2040544

(10) Bonin, J.; Chaussemier, M.; Robert, M.; Routier, M. Homogeneous Photocatalytic Reduction of CO_2 to CO Using Iron (0) Porphyrin Catalysts : Mechanism and Intrinsic Limitations. **2014**, No. 0, 3200–3207. https://doi.org/10.1002/cctc.201402515

(11) Bonin, J.; Robert, M.; Routier, M. Selective and Efficient Photocatalytic CO_2 Reduction to CO Using Visible Light and an Iron Based Homogeneous Cata-. No. Iii, 13–16.

(12) Union, I.; Pure, O. F.; Chemistry, A. Glossary of Terms Used in EFTA. *EFTA Bull.* **1985**, *1* (12), 15–18

(13) Bonin, J.; Robert, M.; Routier, M. Selective and Efficient Photocatalytic CO_2 Reduction to CO Using Visible Light and an Iron-Based Homogeneous Catalyst. **2014**. https://doi.org/10.1021/ja510290t

(14) Appel, A. M.; Bercaw, J. E.; Bocarsly, A. B.; Dobbek, H.; Dubois, D. L.; Dupuis, M.; Ferry, J. G.; Fujita, E.; Hille, R.; Kenis, P. J. A.; et al. Frontiers, Opportunities, and Challenges in Biochemical and Chemical Catalysis of CO_2 Fixation. *Chem. Rev.* **2013**, *113* (8), 6621–6658. https://doi.org/10.1021/cr300463y

(15) Costentin, C.; Robert, M.; Savéant, J. M. Catalysis of the Electrochemical Reduction of Carbon Dioxide. *Chem. Soc. Rev.* **2013**, *42* (6), 2423–2436. https://doi.org/10.1039/c2cs35360a

(16) Qiao, J.; Liu, Y.; Hong, F.; Zhang, J. *A Review of Catalysts for the Electroreduction of Carbon Dioxide to Produce Low-Carbon Fuels*; 2014; Vol. 43.

https://doi.org/10.1039/c3cs60323g

(17) Fontaine, F. G.; Courtemanche, M. A.; Légaré, M. A. Transition-Metal-Free Catalytic Reduction of Carbon Dioxide. *Chem. - A Eur. J.* **2014**, *20* (11), 2990–2996. https://doi.org/10.1002/chem.201304376

(18) Takeda, H.; Ohashi, K.; Sekine, A.; Ishitani, O. Photocatalytic CO_2 Reduction Using Cu(I) Photosensitizers with a Fe(II) Catalyst. **2016**, *1* (I), 50–53. https://doi.org/10.1021/jacs.6b01970

(19) Takeda, H.; Cometto, C.; Ishitani, O.; Robert, M. Electrons, Photons, Protons and Earth-Abundant Metal Complexes for Molecular Catalysis of CO_2 Reduction. *ACS Catal.* **2017**, *7* (1), 70–88. https://doi.org/10.1021/acscatal.6b02181

(20) Concepcion, J. J.; House, R. L.; Papanikolas, J. M.; Meyer, T. J. Chemical Approaches to Artificial Photosynthesis. *Proc. Natl. Acad. Sci.* **2012**, *109* (39), 15560–15564. https://doi.org/10.1073/pnas.1212254109

(21) Muraoka, K.; Kumagai, H.; Eguchi, M.; Ishitani, O.; Maeda, K. A Z-Scheme Photocatalyst Constructed with an Yttrium-Tantalum Oxynitride and a Binuclear Ru(II) Complex for Visible-Light CO_2 Reduction. *Chem. Commun.* **2016**, *52* (50), 7886–7889. https://doi.org/10.1039/c6cc03627a

(22) Gholamkhass, B.; Mametsuka, H.; Koike, K.; Tanabe, T.; Furue, M.; Ishitani, O. Architecture of Supramolecular Metal Complexes for Photocatalytic CO_2 Reduction: Ruthenium-Rhenium Bi- and Tetranuclear Complexes. *Inorg. Chem.* **2005**, *44* (7), 2326–2336. https://doi.org/10.1021/ic048779r

(23) Ishida, H.; Terada, T.; Tanaka, K.; Tanaka, T. Photochemical CO_2 Reduction Catalyzed by $[Ru(Bpy)_2(CO)_2]^{2+}$ Using Triethanolamine and 1 -Benzyl- 1,4-Dihydronicotinamide as

an Electron Donor. *Am. Chem. Soc.* **1990**, 0–6. https://doi.org/https://doi.org/10.1021/ic00330a004

(24) Survey, U. S. G. Rare Earth Elements — Critical Resources for High Technology. **2002**, 1–11.

(25) Schwartz, M.; Vercauteren, M. E.; Sammells, A. F. Fischer-Tropsch Electrochemical CO_2 Reduction to Fuels and Chemicals. **1994**, *141* (11). https://doi.org/10.1149/1.2059287

(26) Schulz, H. Short History and Present Trends of Fischer-Tropsch Synthesis. *Appl. Catal. A Gen.* **1999**, *186* (1–2), 3–12. https://doi.org/https://doi.org/10.1016/S0926-860X(99)00160-X

(27) today, M. D.-C.; 2002, undefined. The Fischer–Tropsch Process: 1950–2000. *Elsevier* **2002**, *71*, 227–241.

(28) Schwarz, H. A.; Dodson, W. Reduction Potentials of CO_2- and the Alcohol Radicals. *J. Phys. Chem.* **1989**, *93* (2), 409–414. https://doi.org/https://doi.org/10.1021/j100338a079

(29) Hawecker, J.; Lehn, J.; Ziessel, R. Photochemical and Electrochemical Reduction of Carbon Dioxide to Carbon Monoxide Mediated by (2,2'-Bipyridine)Tricarbonylchlororhenium(I) and Related Complexes as Homogeneous Catalysts). *Helv. Chim. Acta* **1986**, *69* (1986), 1990. https://doi.org/https://doi.org/10.1002/hlca.19860690824

(30) Takeda, H.; Koike, K.; Inoue, H.; Ishitani, O. Development of an Efficient Photocatalytic System for CO 2 Reduction Using Rhenium (I) Complexes Based on Mechanistic Studies. **2008**, No. I, 6708–6716. https://doi.org/10.1021/ja077752e

(31) Andrade, G. A.; Pistner, A. J.; Yap, G. P. A.; Lutterman, D. A.; Rosenthal, J. Photocatalytic Conversion of CO_2 to CO Using Rhenium Bipyridine Platforms Containing

Ancillary Phenyl or BODIPY Moieties. *ACS Catal.* **2013**, *3* (8), 1685–1692. https://doi.org/10.1021/cs400332y

(32) Ziessel, R.; Hawecker, J.; Lehn, J. Tris(2,2'-Bipyridine)Ruthenium(Ll). *Helv. Chim. Acta* **1986**, *69* (1 986), 1065–1084.

(33) Chen, Z.; Concepcion, J. J.; Brennaman, M. K.; Kang, P.; Norris, M. R.; Hoertz, P. G.; Meyer, T. J. Splitting CO_2 into CO and O_2 by a Single Catalyst. *Proc. Natl. Acad. Sci. U. S. A.* **2012**, *109* (39), 15606–15611. https://doi.org/10.1073/pnas.1203122109

(34) Tamaki, Y.; Morimoto, T.; Koike, K.; Ishitani, O. Photocatalytic CO_2 Reduction with High Turnover Frequency and Selectivity of Formic Acid Formation Using Ru(II) Multinuclear Complexes. *Proc. Natl. Acad. Sci. U. S. A.* **2012**, *109* (39), 15673–15678. https://doi.org/10.1073/pnas.1118336109

(35) Jeletic, M. S.; Mock, M. T.; Appel, A. M.; Linehan, J. C. A Cobalt-Based Catalyst for the Hydrogenation of CO_2 under Ambient Conditions. *J. Am. Chem. Soc.* **2013**, *135* (31), 11533–11536. https://doi.org/10.1021/ja406601v

(36) Ligand, R.; Lacy, D. C.; Mccrory, C. C. L.; Peters, J. C. Studies of Cobalt-Mediated Electrocatalytic CO 2 Reduction Using A. *Inorg. Chem.* **2014**, *53*, 4980–4988.

(37) Froehlich, J. D.; Kubiak, C. P. Homogeneous CO_2 Reduction by Ni(Cyclam) at a Glassy Carbon Electrode. *Inorg. Chem.* **2012**, *51* (7), 3932–3934. https://doi.org/10.1021/ic3001619

(38) Thoi, V. S.; Kornienko, N.; Margarit, C. G.; Yang, P.; Chang, C. J. Visible-Light Photoredox Catalysis: Selective Reduction of Carbon Dioxide to Carbon Monoxide by a Nickel N-Heterocyclic Carbene-Isoquinoline Complex. *J. Am. Chem. Soc.* **2013**, *135* (38), 14413–14424. https://doi.org/10.1021/ja4074003

(39) Wang, D.; Huang, R.; Liu, W.; Sun, D.; Li, Z. Fe-Based MOFs for Photocatalytic CO_2 Reduction: Role of Coordination Unsaturated Sites and Dual Excitation Pathways. *ACS Catal.* **2014**, *4* (12), 4254–4260. https://doi.org/10.1021/cs501169t

(40) Rail, M. D.; Berben, L. A. Directing the Reactivity of $[HFe_4N(CO)_{12}]$? Toward H^+ or CO_2 Reduction by Understanding the Electrocatalytic Mechanism. *J. Am. Chem. Soc.* **2011**, No. Table 1, 18577–18579. https://doi.org/https://doi.org/10.1021/ja208312t

(41) Lian, S.; Kodaimati, M. S.; Dolzhnikov, D. S.; Calzada, R.; Weiss, E. A. Powering a CO_2 Reduction Catalyst with Visible Light through Multiple Sub-Picosecond Electron Transfers from a Quantum Dot. **2017**. https://doi.org/10.1021/jacs.7b03134

(42) Talanquer, V.; Oxtoby, D.; Islam, M. F.; Zhang, J.; Collings, P. J.; Yodh, A. G.; Gleiter, H.; Perepezko, J.; Terrones, M.; Dwyer, J. R.; et al. A Local Proton Source Enhances CO_2 Electroreduction to CO by a Molecular Fe Catalyst. *Science (80-.).* **2012**, No. October, 90–95. https://doi.org/DOI: https://doi.org/10.1126/science.1224581

(43) Rao, H.; Bonin, J.; Robert, M. Non-Sensitized Selective Photochemical Reduction of CO_2 to CO under Visible Light with an Iron Molecular Catalyst. *Chem. Commun.* **2017**, *53* (19), 2830–2833. https://doi.org/10.1039/c6cc09967j

(44) Lorimer, J. W.; Clever, H. L.; Young, C. L. Carbon Dioxide in Non–Aqueous Solvents At Pressures Less Than 200 KPA, IUPAC Solubility Data Series. **1992**, *50*. https://doi.org/10.1016/B978-0-08-040495-0.50007-5

(45) Bhugun, I.; Lexa, D.; Savéant, J. M. Catalysis of the Electrochemical Reduction of Carbon Dioxide by Iron(0) Porphyrins: Synergystic Effect of Weak Brönsted Acids. *J. Am. Chem. Soc.* **1996**, *118* (7), 1769–1776. https://doi.org/10.1021/ja9534462

(46) PubChem. National Center for Biotechnology Information. PubChem Database. Dipyrrin,

CID=3083424, https://pubchem.ncbi.nlm.nih.gov/compound/Dipyrrin (accessed on Jan. 28, 2020).

(47) Wang, H.; Fronczek, F. R.; Vicente, M. G. H.; Smith, K. M. Functionalization of 3,5,8-Trichlorinated BODIPY Dyes. *J. Org. Chem.* **2014**, *79* (21), 10342–10352. https://doi.org/10.1021/jo501969z

(48) Bañuelos, J.; Arroyo-Córdoba, I. J.; Valois-Escamilla, I.; Alvarez-Hernández, A.; Peña-Cabrera, E.; Hu, R.; Zhong Tang, B.; Esnal, I.; Martínez, V.; López Arbeloa, I. Modulation of the Photophysical Properties of BODIPY Dyes by Substitution at Their Meso Position. *RSC Adv.* **2011**, *1* (4), 677–684. https://doi.org/10.1039/c1ra00020a

(49) Lincoln, R.; Greene, L. E.; Krumova, K.; Ding, Z.; Cosa, G. Electronic Excited State Redox Properties for BODIPY Dyes Predicted from Hammett Constants: Estimating the Driving Force of Photoinduced Electron Transfer. *J. Phys. Chem. A* **2014**, *118* (45), 10622–10630. https://doi.org/10.1021/jp5059148

(50) Wood, T. E.; Thompson, A. Advances in the Chemistry of Dipyrrins and Their Complexes. **2007**. https://doi.org/10.1021/cr050052c

(51) Hanson, K.; Tamayo, A.; Diev, V. V.; Whited, M. T.; Djurovich, P. I.; Thompson, M. E. Efficient Dipyrrin-Centered Phosphorescence at Room Temperature from Bis-Cyclometalated Iridium(III) Dipyrrinato Complexes. *Inorg. Chem.* **2010**, *49* (13), 6077–6084. https://doi.org/10.1021/ic100633w

(52) McLean, T. M.; Moody, J. L.; Waterland, M. R.; Telfer, S. G. Luminescent Rhenium(I)-Dipyrrinato Complexes. *Inorg. Chem.* **2012**, *51* (1), 446–455. https://doi.org/10.1021/ic201877t

(53) Cohen, S. M.; Halper, S. R. Dipyrromethene Complexes of Iron.Pdf. Elsevier: San Diego

2002. https://doi.org/https://doi.org/10.1016/S0020-1693(02)01176-3

(54) Gupta, R. K.; Yadav, M.; Pandey, R.; Pandey, D. S. Synthesis and Characterization of Some Heteroleptic Copper(II) Complexes Based on Meso-Substituted Dipyrrins. *J. Chem. Sci.* **2011**, *123* (6), 819–826. https://doi.org/10.1007/s12039-011-0169-1

(55) Hewat, T. E.; Yellowlees, L. J.; Robertson, N. Neutral Copper(i) Dipyrrin Complexes and Their Use as Sensitizers in Dye-Sensitized Solar Cells. *Dalt. Trans.* **2014**, *43* (10), 4127–4136. https://doi.org/10.1039/c3dt53334d

(56) Trinh, C.; Kirlikovali, K.; Das, S.; Ener, M. E.; Gray, H. B.; Djurovich, P.; Bradforth, S. E.; Thompson, M. E. Symmetry-Breaking Charge Transfer of Visible Light Absorbing Systems: Zinc Dipyrrins. *J. Phys. Chem. C* **2014**, *118* (38), 21834–21845. https://doi.org/10.1021/jp506855t

(57) Bartynski, A. N.; Gruber, M.; Das, S.; Rangan, S.; Mollinger, S.; Trinh, C.; Bradforth, S. E.; Vandewal, K.; Salleo, A.; Bartynski, R. A.; et al. Symmetry-Breaking Charge Transfer in a Zinc Chlorodipyrrin Acceptor for High Open Circuit Voltage Organic Photovoltaics. *J. Am. Chem. Soc.* **2015**, *137* (16), 5397–5405. https://doi.org/10.1021/jacs.5b00146

(58) Tungulin, D.; Leier, J.; Carter, A. B.; Powell, A. K.; Albuquerque, R. Q.; Unterreiner, A. N.; Bizzarri, C. Chasing BODIPY: Enhancement of Luminescence in Homoleptic Bis(Dipyrrinato) Zn II Complexes Utilizing Symmetric and Unsymmetrical Dipyrrins. *Chem. - A Eur. J.* **2019**, *25* (15), 3816–3827. https://doi.org/10.1002/chem.201806330

(59) Sazanovich, I. V.; Kirmaier, C.; Hindin, E.; Yu, L.; Bocian, D. F.; Lindsey, J. S.; Holten, D. Structural Control of the Excited-State Dynamics of Bis(Dipyrrinato)Zinc Complexes: Self-Assembling Chromophores for Light-Harvesting Architectures. *J. Am. Chem. Soc.* **2004**, *126* (9), 2664–2665. https://doi.org/10.1021/ja038763k

(60) Alqahtani, N. Z.; Blevins, T. G.; McCusker, C. E. Quantifying Triplet State Formation in Zinc Dipyrrin Complexes. *J. Phys. Chem. A* **2019**. https://doi.org/10.1021/acs.jpca.9b08682

(61) Azcarate, I.; Costentin, C.; Robert, M.; Savéant, J. M. Dissection of Electronic Substituent Effects in Multielectron-Multistep Molecular Catalysis. Electrochemical CO_2-to-CO Conversion Catalyzed by Iron Porphyrins. *J. Phys. Chem. C* **2016**, *120* (51), 28951–28960. https://doi.org/10.1021/acs.jpcc.6b09947

(62) Costentin, C.; Robert, M.; Savéant, J. M. Current Issues in Molecular Catalysis Illustrated by Iron Porphyrins as Catalysts of the CO_2-to-CO Electrochemical Conversion. *Acc. Chem. Res.* **2015**, *48* (12), 2996–3006. https://doi.org/10.1021/acs.accounts.5b00262

(63) Azcarate, I.; Costentin, C.; Robert, M.; Savéant, J. M. Through-Space Charge Interaction Substituent Effects in Molecular Catalysis Leading to the Design of the Most Efficient Catalyst of CO_2-to-CO Electrochemical Conversion. *J. Am. Chem. Soc.* **2016**, *138* (51), 16639–16644. https://doi.org/10.1021/jacs.6b07014

(64) Lian, S.; Kodaimati, M. S.; Dolzhnikov, D. S.; Calzada, R.; Weiss, E. A. Powering a CO_2 Reduction Catalyst with Visible Light through Multiple Sub-Picosecond Electron Transfers from a Quantum Dot. *J. Am. Chem. Soc.* **2017**, *139* (26), 8931–8938. https://doi.org/10.1021/jacs.7b03134

(65) Alqahtani, N. Synthesis and Characterization of Zinc(II) Dipyrrin Photosensitizers. **2018**, No. Ii.

(66) Pellegrin, Y.; Odobel, F. Les Donneurs d'électron Sacrificiels Pour La Production de Combustible Solaire. *Comptes Rendus Chim.* **2017**, *20* (3), 283–295. https://doi.org/10.1016/j.crci.2015.11.026

(67) Mohamed, E. A.; Zahran, Z. N.; Naruta, Y. Efficient Electrocatalytic CO_2 Reduction with a Molecular Cofacial Iron Porphyrin Dimer. *Chem. Commun.* **2015**, *51* (95), 16900–16903. https://doi.org/10.1039/c5cc04273a

(68) Narayanan, M.; Kodali, G.; Singh, V. R.; Velvadapu, V.; Stanley, R. J. Oxidation and Reduction Potentials of 8-Vinyladenosine Measured by Cyclic Voltammetry: Implications for Photoinduced Electron Transfer Quenching of a Fluorescent Adenine Analog. *J. Photochem. Photobiol. A Chem.* **2012**, *249*, 9–14. https://doi.org/10.1016/j.jphotochem.2012.08.018

(69) Elgrishi, N.; Rountree, K. J.; McCarthy, B. D.; Rountree, E. S.; Eisenhart, T. T.; Dempsey, J. L. A Practical Beginner's Guide to Cyclic Voltammetry. *J. Chem. Educ.* **2018**, *95* (2), 197–206. https://doi.org/10.1021/acs.jchemed.7b00361

(70) Sakamoto, R.; Iwashima, T.; Kögel, J. F.; Kusaka, S.; Tsuchiya, M.; Kitagawa, Y.; Nishihara, H. Dissymmetric Bis(Dipyrrinato)Zinc(II) Complexes: Rich Variety and Bright Red to near-Infrared Luminescence with a Large Pseudo-Stokes Shift. *J. Am. Chem. Soc.* **2016**, *138* (17), 5666–5677. https://doi.org/10.1021/jacs.6b02128

(71) Inzelt, G.; Lewenstam, A.; Scholz, F. *György Inzelt Handbook of Reference Electrodes*; 2013. https://doi.org/10.1007/978-3-642-36188-3

(72) Azcarate, I.; Costentin, C.; Robert, M.; Savéant, J. M. Dissection of Electronic Substituent Effects in Multielectron-Multistep Molecular Catalysis. Electrochemical CO_2-to-CO Conversion Catalyzed by Iron Porphyrins. *J. Phys. Chem. C* **2016**, *120* (51), 28951–28960. https://doi.org/10.1021/acs.jpcc.6b09947

(73) Skoog, D.; Holler, J.; Crouch, S. *Principles of Instrumental Analysis*, Seventh ed.; Cengage learning, 2018.

(74) Chauvin, J.; Lafolet, F.; Chardon-noblat, S.; Deronzier, A. Towards New Molecular Photocatalysts for CO 2 Reduction : Photo-Induced Electron Transfer versus CO Dissociation within [Os(NN)(CO)$_2$Cl$_2$]. **2011**, 4313–4322. https://doi.org/10.1002/chem.201003098

VITA

SENAN ADNAN RASHEED

Education: M.S. Chemistry, East Tennessee State University, Johnson City, Tennessee, 2020

B.Sc. Chemistry, Sam Houston State University, Huntsville, Texas, 2013

Professional Experience: Graduate Assistant, East Tennessee State University, College of Arts and Sciences, 2017-2020

Quality Control Chemist, Emirates National Oil Company, 2014-2015

Lab research assistant, Sam Houston State University, 2010-2013

Publications: Yu, J. C.C., (2012) "Formulation studies on selected water insoluble sulfur donor used in fighting cyanide antagonism." *TAS Meeting*, Alpine, TX.

Shifflet, M., (2012) "Preclinical Drug Formulation and Animal Studies in Cyanide Antidote Development." *Fifth Annual Undergraduate Research Symposium*, Huntsville, TX.

Winner, B.M., (2011) "Micellar Encapsulation of Sulfur Donors to Combat Cyanide Antagonism." *ACS,* Austin, TX

Negrito, M., (2011) “Recombinant Human Rhodanese in Cyanide Antagonism. *ACS,* Austin, TX

Duke, A., (2012) “Solubility Enhancement for a Poorly Water-Soluble Drug.” *ACS,* Baton Rouge, LA.

Rasheed, S., (2013) “Solubility studies using co-solvent system combinations for a poorly water-soluble drug.” *TAS Meeting*, Philadelphia, PA

Kovacs, K., (2014) “Identification, Solubility enhancement and in vivo testing of a cyanide antidote.” *European Journal of Pharm. Sci*.

Honors and Awards: Robert Welch Research Fellowship (2011)

US Army Summer Research Award, Sam Houston State University, (2012)